Fine and hyperfine resolved empirical energy levels of VO

Charles A. Bowesman, Hanieh Akbari, W.Scott Hopkins, Sergei N. Yurchenko, Jonathan Tennyson

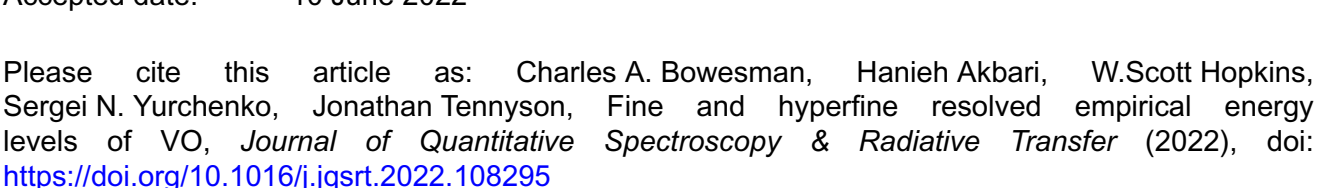
PII: \$0022-4073(22)00230-8

DOI: https://doi.org/10.1016/j.jqsrt.2022.108295

Reference: JQSRT 108295

To appear in: Journal of Quantitative Spectroscopy & Radiative Transfer

Received date: 10 March 2022 Revised date: 17 May 2022 Accepted date: 10 June 2022



This is a PDF file of an article that has undergone enhancements after acceptance, such as the addition of a cover page and metadata, and formatting for readability, but it is not yet the definitive version of record. This version will undergo additional copyediting, typesetting and review before it is published in its final form, but we are providing this version to give early visibility of the article. Please note that, during the production process, errors may be discovered which could affect the content, and all legal disclaimers that apply to the journal pertain.

© 2022 Published by Elsevier Ltd.



Highlights

- A MARVEL analysis of 6 quartet and 7 doublet states of VO yields 4641 empirical energy levels
- A separate analysis of hyperfine-resolved transitions gives 4393 levels with hyperfine structure
- 191 lines are assigned the 2 X intercombination band system



Fine and hyperfine resolved empirical energy levels of VO

Charles A. Bowesman^a, Hanieh Akbari^a, W. Scott Hopkins^b, Sergei N. Yurchenko^a, Jonathan Tennyson^{a,*}

^aDepartment of Physics and Astronomy, University College London, Gower Street, London WC1E 6BT, UK
^bDepartment of Chemistry, University of Waterloo, Waterloo, Ontario N2L 3G1, Canada

Abstract

A MARVEL (measured active rotational-vibrational energy levels) analysis of the spectra of vanadium oxide (VO) is performed, involving thirteen electronic states (6 quartets and 7 doublets). $^{51}V^{16}O$ data from 14 sources are used to form three networks: hyperfine-resolved quartets, hyperfine-unresolved quartets and hyperfine-unresolved doublets. A single quartet network is formed by deperturbing the hyperfine lines and 191 lines are assigned to an intercombination $2\,^2\Pi$ –X $^4\Sigma^-$ band system in the visible region previously recorded by Hopkins et al. (J. Chem. Phys. 130 (2009) 144308), allowing the doublet and quartet networks to be merged. As a result 6 603/4 402 validated transitions/final energies were obtained from analysis of the hyperfine-resolved network and 9 087/4712 from the unresolved. T_v energy values and other molecular constants are determined for all doublet states within the networks.

Keywords: molecular data - opacity - planets and satellites: atmospheres - stars: atmospheres - ISM: molecules.

1. Introduction

The spectrum of Vanadium oxide (VO) is of astrophysical significance in several areas, such as in late M [1–11] and early L [12, 13] dwarfs and subdwarfs where it is known to be a significant opacity source and characterises their spectra with strong absorption features. The same features have been observed in late-type Mira variables [14–16] and arise primarily from vibronic transitions in the A $^4\Pi$ –X $^4\Sigma$ –, B $^4\Pi$ –X $^4\Sigma$ – and C $^4\Sigma$ –X $^4\Sigma$ – bands [8]. The C $^4\Sigma$ –X $^4\Sigma$ – absorption band has also been observed in the nova of V838 Mon [17] and a B $^4\Pi$ –X $^4\Sigma$ – emission band was observed in the nova–like eruption of V4332 Sgr [18].

It is thought that VO also plays an important role in determining the structure of and driving temperature inversion in the atmospheres of hot Jupiter exoplanets [19–23]. Studies have looked to confirm these effects in the hot Jupiters WASP-121b [24–27] and HD 209458b but evidence has been tentative [20, 28, 29].

The ExoMol group provided a high temperature rovibronic line list for VO, dubbed VOMYT after the species and three author's initials [30]. The line list was generated using potential energy curves and couplings based on initial *ab initio* electronic structure calculations which were then tuned using experimental data; the program Duo [31] was used to solve the variational nuclear motion problem. VOMYT considers transitions between the 13 lowest electronic states of VO which are a mixture of the doublet and quartet spin states. VO is a challenging system to treat using *ab initio* methods [32] and consequently VOMYT is not accurate enough for high-resolution astronomical studies

*Corresponding author.

Email address: j.tennyson@ucl.ac.uk (Jonathan Tennyson)

[33]; one aim of the present work is to provide a better dataset for such studies.

One issue we address directly in this paper is the separation between the doublet and quartet states. Hopkins *et al.* [34] recorded an intercombination $2^2\Pi - X^4\Sigma^-$ band spectrum for VO. We present here a series of new assignments to spectra of the $2^2\Pi - X^4\Sigma^-$ bands originally published by Hopkins *et al.* which allow us to connect doublet and quartet states in a single spectroscopic network.

Another issue is the treatment of hyperfine effects. Considering 51 V 16 O: while 16 O has zero nuclear spin 51 V has $I=\frac{7}{2}$ leading to large hyperfine splittings. The hyperfine splitting of VO electronic spectra has been known to significantly contribute to the appearance of its spectra for some time [35] with hyperfine structures that can spread a transition over more than 1 cm $^{-1}$. These splittings are largest in the X $^{4}\Sigma^{-}$ ground state which result in substantially blended spectra for any bands involving this state when observed below hyperfine resolution [36]. This means that it is not possible to consider a high-resolution spectrum of VO without at least for some parts of it accounting for hyperfine effects. In this work we present networks of both hyperfine-resolved and hyperfine-unresolved transitions.

Fig. 1 details the known and predicted low-lying electronic states of VO, showing those considered explicitly in this study. One further issue is that the density of these states leads to many local perturbations due to interactions between various electronic states and interactions between the hyperfine states of different fine structure components. While we do not attempt an exhaustive analysis of these various perturbations, they are noted and catalogued.

The paper is organized as follows. Section 2 briefly presents the MARVEL (measured active rotational-vibrational energy levels) and our hyperfine deperturbation procedure. Section 3

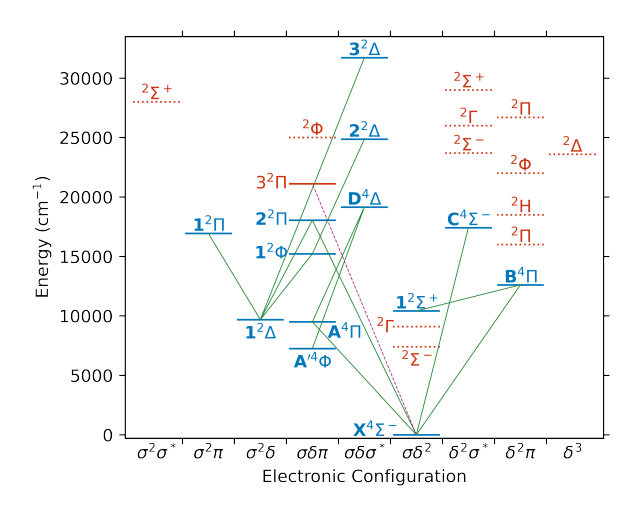


Fig. 1: The electronic states of VO by electronic configuration: solid black horizontal lines represent states that have been observed, while those that are dotted are predicted by electronic structure calculations. Electronic states contained within the new MARVEL networks presented here are given in blue, while those not in the network are in red. Solid green lines represent transitions between states that are included within our networks, while dashed purple lines are transitions that have not been included as they are yet to be fully assigned.

describes the transition data used including the new spectral assignments. Section 4 presents our MARVEL results for both hyperfine-resolved and hyperfine-unresolved networks. Section 5 gives our conclusion and discusses anticipated further work.

2. Method

2.1. MARVEL overview

The MARVEL procedure [37] allows for the inversion of heterogeneous datasets of transitions from high-resolution spectroscopic experiments to give empirical energy levels with associated uncertainties [37–39]. MARVEL constructs spectroscopic networks consisting of energy levels as nodes and transitions as edges [40]. These networks are constructed from an input list of assigned transitions that connect an upper and lower energy level.

As the Marvel procedure determines empirical energies for the levels connected by observed transitions, it also enables the determination of energy differences between levels that have no observed transitions between them [41]. Hence it allows us to calculate the transition frequency for any possible transition between any levels contained within the Marvel network. For example, applying this technique to formaldehyde allowed for the determination of 367 779 transition frequencies from the empirical energy levels derived from 16 403 observational transitions [42]. Additionally, provided the experimental uncertainties in the transition data are set appropriately, the use of Marvel avoids having to treat effects such as perturbations or resonances separately, i.e.: with effective Hamiltonians. Put simply the Marvel procedure does not require any underlying spectroscopic model for the system as Marvel treats each level

as a node within the network, rather than addressing the physics implied by the quantum numbers assigned to it. Given the large number of perturbations known to occur in the spectra of VO, this approach avoids a considerable number of additional calculations.

Each transition comprises of a transition frequency (in cm⁻¹) with accompanying uncertainty, an associated tag to identify the transition and a full set of upper and lower state quantum numbers. The set of quantum numbers chosen to identify a given state is configurable but must be uniform throughout the whole network. In this work, each state was labelled by its electronic state term symbol, a fine structure configuration $(F_1,$ F_2 , F_3 or F_4), the projection of the total electronic angular momentum Ω , total parity (+/-), vibrational quantum number v and total angular momentum quantum number J. Observed VO transitions involve states best described by Hund's case (b) couplings in the observed $\Lambda = 0$, $^4\Sigma^-$ and $^2\Sigma^+$ states, including the ground state, or by case (a) coupling otherwise. Even where case (b) is used however, there are instances at low J where this breaks down and is better described by case (a) [43]. Because of this, both Ω and fine structure are provided even though they are in most cases synonymous.

Hyperfine-resolved transitions are also identified by the additional quantum number F, the result of the coupling of Jand the nuclear spin I. As MARVEL requires all states to have the same set of quantum number labels, these F values must be removed or these transitions separated into another network. Noting that there are no assigned intercombination bands in the literature and none of the doublet state transitions have been observed hyperfine-resolved, we initially constructed three networks. Network 1 comprised all hyperfine-resolved quartet transitions; network 2 contained hyperfine-unresolved quartets and network 3 contained the (hyperfine-unresolved) doublet transitions. The rest of this section describes our approach for deperturbing the hyperfine-resolved transitions allowing a single quartet network to be built. Section 3.2 discusses our assignments of the 2 ${}^{2}\Pi$ -X ${}^{4}\Sigma$ - band system spectra which allowed us to create a single, unified network of hyperfine-unresolved transitions. At the same time we also use our hyperfine-resolved quartet transitions to give hyperfine-resolved empirical energy levels.

2.2. Hyperfine deperturbation

We considered using effective Hamiltonian calculations to determine additional hyperfine-unresolved transition frequencies by using molecular constants from fits to hyperfine-resolved data. This would allow us to expand the coverage of our hyperfine-unresolved marvel network to regimes only connected to via hyperfine-resolved transitions. Moreover, the high accuracy of the hyperfine transition measurements should allow for high-accuracy constants to be determined and hence high-accuracy transitions frequencies to be determined. However, setting the hyperfine constants to zero in order to calculate hyperfine-unresolved transition frequencies does not necessarily produce accurate results. To test the effectiveness of this method, we used constants from fits to hyperfine-resolved data for the X $^4\Sigma^-$ [44], B $^4\Pi$ [45] and C $^4\Sigma^-$ [43] states to calculate

transition frequencies for comparison. Using the program PGO-PHER [46] to carry out the effective Hamiltonian calculations, we generated a set of transition frequencies for every possible $\Delta J = \pm 1.0$ transition up to J' = 99.5 in the B $^4\Pi$ -X $^4\Sigma$ -(0,0) and C $^4\Sigma^-$ – X $^4\Sigma^-$ (0,0) bands. These calculated frequencies were checked against their published hyperfine-unresolved counterparts [45, 47] for consistency. Out of the 896 observed transitions in these bands, only 97 had their frequencies accurately recreated by the effective Hamiltonian calculations. We note that the hyperfine constants are not uncorrelated with the other effective Hamiltonian constants used in the fit and therefore removing hyperfine parameters will not generally lead to same result as fitting without them. Hence, this approach was deemed inadequate for our high-resolution study and an alternative method of deperturbing the hyperfine-resolved transitions was adopted.

In this work, we refined deperturbation techniques that had been previously implemented elsewhere for incorporating hyperfine-resolved data into hyperfine-unresolved MARVEL networks to supplement their energy level coverage [48, 49]. When deperturbing hyperfine components into a single transition, hyperfine transitions are only combined with others from the same data source. This is to ensure that any systematic effects that might be present in the data of a given source do not pollute the data of other sources. It is left to the MARVEL procedure to subsequently evaluate the validity of multiple sources of data in combination.

To carry out the deperturbation, a weighted mean transition frequency is determined. This is done to simulate how these hyperfine transitions would combine into a single spectral feature at a lower resolution and as such are weighted by their intensities. As no transition intensities are measured however, relative values are calculated using a method previously applied by Fast and Meek [50] to hyperfine transitions of SH and similarly to update the ExoMol line list for AlO [51]:

$$I(F',F'',J'',J',I) \propto (2F'+1)(2F''+1) \begin{cases} F' & F'' & 1 \\ J'' & J' & I \end{cases}^2. (1)$$

This form is derived from the square of the reduced matrix element of the electric dipole moment and can be readily found in the literature [52–55]. This expression relies on there being no additional coupling between angular momenta and hence cannot be used for transitions with $|\Delta J| > 1$, such as O- or S-branch transitions, which would violate the triangle condition on the (J'', J', 1) triad in the above 6j-symbol. All other terms that do not depend on F' or F'' will be equal for all hyperfine components of a given transition and as such can be disregarded when comparing their relative intensities. We note that including O-and S-branch transitions when deperturbing would not have led to the characterization of any extra energy levels.

2.3. Deperturbation uncertainty scaling

We provide uncertainty estimates for our deperturbed transitions that are the product of a base uncertainty and three scale factors. The base uncertainty is the standard error propagation of the weighted mean of the uncertainties of the deperturbed hyperfine transitions. Each transition has a normalised weight w_i

defined as the respective transition's relative intensity, calculated using Eq. (1), as a fraction of the total intensity of all hyperfine components being deperturbed. Given a set of hyperfine transitions with individual transition wavenumber uncertainties $\Delta \tilde{v}_i$, the intensity weighted mean uncertainty is defined by:

$$\Delta \tilde{v}_{\text{iwm}} = \left(\sum_{i=1}^{n} w_i^2 \Delta \tilde{v}_i^2\right)^{\frac{1}{2}}.$$
 (2)

The first scale factor considers the completeness of the subset of hyperfine transitions present in our data. To assess this, we first determine what constitutes the full set of possible hyperfine transitions that we can expect to be observed between the upper and lower states. Though F obeys the selection rule $\Delta F = \pm 1, 0$, not all of these ΔF components will be observed due to the propensity rule which suggests that $\Delta F = \Delta J$ transitions are strongly favoured. There are of course exceptions to this rule and most hyperfine-resolved sources report a considerable number of $\Delta F \neq \Delta J$ transitions at low J values [43–45, 56]. For each set of hyperfine transitions that we deperturb we assess the set of ΔF values that are present, $\Delta F_{\rm pres}$, and can hence determine the total possible number of hyperfine transitions with the corresponding ΔF values. We chose to determine this for each transition individually to avoid attempting to define a cut-off value for J above which we no longer consider $\Delta F \neq \Delta J$ transitions as this did not appear to be consistent between different sources, varying dependent on their ability to resolve low-intensity lines.

Considering a transition between two levels with total angular momentum quantum J_{max} and J_{min} ($J_{\text{max}} \geq J_{\text{min}}$): the number of possible hyperfine components of the transition, n_{poss} , is limited by J_{min} . The possible number of hyperfine configurations, i.e., the possible values of F are given by the relationship F = J + I, such that the number of possible hyperfine configurations for a given level is $n_{\text{hf}}(J) = J + I - |J - I| + 1$. If $J \geq I$ this simplifies to the expected 2I + 1. When J < I however, this value is reduced by 2 for each integer decrease in J below the value of I. We calculate n_{poss} given the values of ΔF in the set ΔF_{poss} with the following relationship:

$$n_{\text{poss}} = \begin{cases} \sum_{\Delta F_{\text{poss}}} n_{\text{hf}} (J_{min}), & \text{if } J_{\text{min}} < J_{\text{max}} \le I \\ \sum_{\Delta F_{\text{poss}}} (n_{\text{hf}} (J_{min}) - |\Delta J - \Delta F|), & \text{otherwise.} \end{cases}$$
(3)

An additional case exists in Eq. (3), when $J_{\min} < I < J_{\max}$. Given both I and J are half-integer for VO however, J_{\min} and J_{\max} must differ by more than 1 to satisfy this condition. This can occur for O- and S-branch transitions, but these are excluded from our deperturbation process due to the $|\Delta J| \le 1$ condition implied by Eq. (1).

Once n_{poss} has been calculated, it is compared against the real number of hyperfine transitions present within our data set that are to be deperturbed into a single transition, n_{pres} . These are combined into the uncertainty scale factor $\Delta \tilde{v}_{\text{pres}}$ with a constant a=4 such that there is a 5-fold increase to the base uncertainty when only one hyperfine transition is present. There

is no uncertainty increase from this factor when all possible hyperfine transitions are present ($\Delta \tilde{v}_{pres} = 1$):

$$\Delta \tilde{v}_{\rm pres} = 1 + a \times \frac{n_{\rm poss} - n_{\rm pres}}{n_{\rm poss} - 1}. \tag{4}$$

The term $\Delta \tilde{v}_{pres}$ provides the smallest uncertainty increase of the scale factors we consider here.

The second uncertainty scale factor we employ accounts for the distribution of the subset of hyperfine transitions present in our data, whereby we look to see if the values of F are evenly distributed about J or skewed to one side. To calculate this, we again consider the set of possible hyperfine transitions that we expect to observe between the given upper and lower energy levels, accounting for the present values of ΔF_{pres} . For each transition, we take the mean value of the hyperfine quantum number in the upper and lower state to give us a 'centre' value, $F_{\rm c}$. It is important to consider that this $F_{\rm c}$ term is not a quantum number for either upper or lower level but rather a metric for measuring the relative positions of hyperfine transitions. We then take the mean of this centre for all possible transitions, $\overline{F}_{c,poss}$. The same calculation is also performed for the subset of hyperfine transitions present in our data and we take the magnitude of the difference between these two values as the measure of the distribution of our hyperfine transitions:

$$\Delta \tilde{v}_{\text{dist}} = 1 + b \times |\overline{F}_{\text{c,poss}} - \overline{F}_{\text{c,pres}}|. \tag{5}$$

The maximum value of the difference between the two \overline{F}_c terms is I, occurring when only one hyperfine transition is present that has either $F = J \pm I$ in both upper and lower energy levels. Given this fact, the value of b was set to 4 such that this term produces the largest scaling of uncertainty when the distribution of transitions is most uneven.

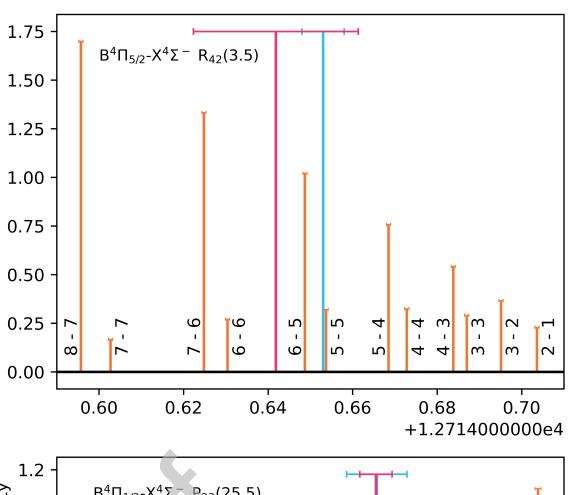
The derived scaling terms from Eq. (4) and Eq. (5) are combined with the initial propagated uncertainty and a final scale factor c to determine the final deperturbed uncertainty, $\Delta \tilde{v}_{\rm dpt}$:

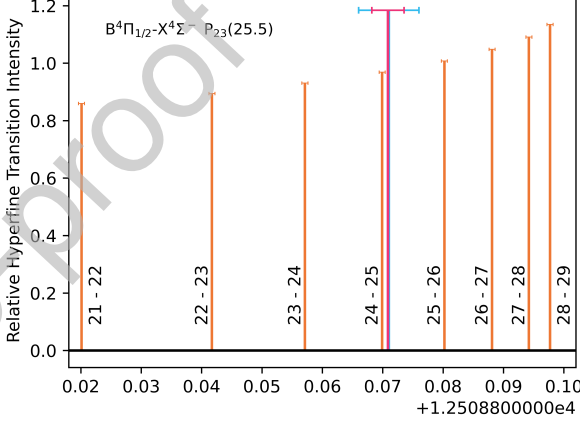
$$\Delta \tilde{v}_{\rm dpt} = c \times \Delta \tilde{v}_{\rm iwm} \times \Delta \tilde{v}_{\rm pres} \times \Delta \tilde{v}_{\rm dist}. \tag{6}$$

The scale factor c was set to 15 based on direct comparisons between the final energy of the deperturbed hyperfine transitions and equivalently assigned, hyperfine-unresolved transitions also considered in this work. This value was chosen such that at least one standard deviation of matching, equivalent transitions were consistent in their energies. In total, 269 matching transitions were found between the deperturbed hyperfine and hyperfine-unresolved data; 173 B $^4\Pi$ -X $^4\Sigma$ - [45] and 96 C $^4\Sigma$ --X $^4\Sigma$ - [47] transitions. This process is illustrated in Fig. 2.

3. Experimental data sources

The electronic structure of VO has been discussed at great length in the literature over the years [36, 57–75]. This substantial coverage ensured any outdated transition assignments relating to fine structure or electronic state designation present in older sources could easily be updated and relabelled using our





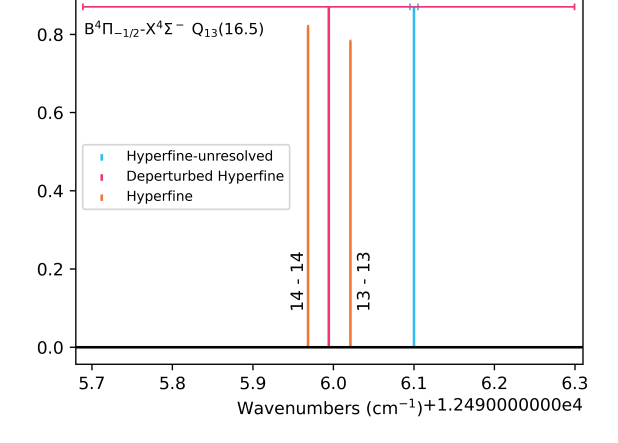


Fig. 2: Comparisons between the deperturbed hyperfine line centres calculated using the relative intensity weighted mean and the observed hyperfine-unresolved line centres for three B $^4\Pi$ –X $^4\Sigma^-$ (0,0) transitions within our data set. The constituent hyperfine transitions that were used to calculate the deperturbed line centres are overlaid, labelled with their F' and F'' values. Top panel: example involving observed hyperfine transitions with multiple ΔF values; the transitions with $\Delta F \neq \Delta J$ are predicted to be much weaker. Middle: case where full set of $\Delta F = \Delta J$ hyperfine transitions are available, resulting in very close deperturbed and hyperfine-unresolved line centres. Bottom: case with skewed distribution of hyperfine transitions, resulting in a deperturbed line centre that is not very consistent with the observed hyperfine-unresolved equivalent. The uncertainties in the individual hyperfine transitions are all $0.005 \, \mathrm{cm}^{-1}$ which is too small to be seen on the scale of the bottom panel.

specified quantum numbers. Some sources that were considered when collecting data to build our spectroscopic networks were ultimately not included, either because their reported transitions did not include complete assignments or because their transitions were only reported qualitatively and without individual transitions wavenumbers [76-80]. Others exclusively report measurements of perturbed transitions where the perturbing state has not been identified [81]. Multiple data sources report transitions affected by the internal hyperfine perturbations arising from a crossing between the F_2 and F_3 fine structure components discovered by Richards & Barrow [78]. With experimental data that is hyperfine resolved it is possible to fully assign such perturbations, but there are instances of Dopplerlimited observations where these internal hyperfine perturbations have been observed [45, 82]. We differentiate internal hyperfine and unconfirmed electronic state perturbations in the MARVEL input file by appending '_PH' and '_PE' respectively to the end of the electronic state label.

3.1. MARVELISED data sources

The following 14 data sources provide data that are included in the new spectroscopic networks described by this paper:

57LaSe: Lagerqvist and Selin [47] report 1168 measured R- and P-branch C $^4\Sigma^-$ –X $^4\Sigma^-$ transitions, 28 of which are perturbed by an unconfirmed electronic state. These branches are provided with the subscripts 'a' and 'b' in place of fine structure notation as this was not explicitly determined in their original work. We confirmed that these subscripts corresponded to the F_3 and F_2 fine structure components respectively through the analysis of combination differences and by checking their consistency with the rest of the MARVEL network.

81HoMeMi: Hocking *et al.* [83] provide 48 hyperfineresolved C $^4\Sigma^-$ -X $^4\Sigma^-$ transition measurements.

82ChHaMe: Cheung *et al.* [43] provide measurements for 2 834 hyperfine-resolved C $^4\Sigma^-$ –X $^4\Sigma^-$ transitions, 17 of which are perturbed by an unconfirmed electronic state. Their observations included a number of internal hyperfine perturbations which they were able to fully assign.

82ChTaMe: Cheung *et al.* [82] report 1 058 A $^4\Pi$ –X $^4\Sigma$ ⁻ transition measurements, 7 of which exhibit internal hyperfine perturbations.

87MeHuChTa: Merer *et al.* [84] provide 1 289 measurements for transitions involving quartet states, split between the D $^4\Delta$ -A' $^4\Phi$ (980 transitions, 2 of which are perturbed) and D $^4\Delta$ -A $^4\Pi$ (309) bands. They also give measurements for 1 139 doublet transitions split between the 1 $^2\Pi$ -1 $^2\Delta$ (885), 2 $^2\Pi$ -1 $^2\Delta$ (81) and 2 $^2\Delta$ -1 $^2\Phi$ (173) bands. Of these, 744 quartet and 411 doublet transitions are reported with unresolved Λ -doubling and hence had no parity assignment. Such transitions were entered into the MARVEL input file twice with both applicable upper and lower state total parity (+/-) combinations.

91SuFrLoGi: Suenram *et al.* [56] report three very high accuracy measurements of hyperfine transitions within the X $^4\Sigma^-$ ground state.

94ChHaHuHu: Cheung *et al.* [85] provide measurements for 471 B $^4\Pi$ -X $^4\Sigma$ - transitions, 7 of which are perturbed by the 1 $^2\Sigma$ +, v=3 state.

95AdBaBeBo: Adam *et al.* [45] provide two sets of data: 3 534 hyperfine-resolved and 776 hyperfine-unresolved B $^4\Pi$ - X $^4\Sigma^-$ transitions. 14 of the hyperfine-resolved and 8 of the hyperfine-unresolved transitions are perturbed by the 1 $^2\Sigma^+$, v=2 state, in addition to 22 further hyperfine-unresolved transitions perturbed by an unknown state.

97KaLiLuSa: Karlsson *et al.* [86] report 47 measured A ${}^4\Pi$ -X ${}^4\Sigma$ - transitions.

02RaBeDaMe: Ram *et al.* [87] provide 218 measurements of transitions in the 1 $^2\Phi$ -1 $^2\Delta$ band with no observed Λ -doubling and hence no parity assignment. As with the data from 87MeHuChTa [84], these transitions were each entered twice with both applicable upper and lower state parity combinations.

05RaBe: Ram and Bernath [88] report 166 transitions in the 3 2 Δ-1 2 Δ band with no observed Λ-doubling. Again, each transition was input twice with both applicable upper and lower state parity combinations.

08FlZi: Flory and Ziurys [44] report 224 ground state, pure rotation X $^4\Sigma^-$ Ay hyperfine transitions. They observed the effects of the same internal hyperfine perturbation described by other sources but were able to fully assign the affected transitions. Four of these very high-accuracy transitions were inconsistent with hyperfine transitions from 82ChHaMe [43] and 95AdBaBeBo [45]. Through comparisons with current hyperfine calculations [89] we determined that it was the four transitions from this source that were incorrect and had likely been misassigned.

08SrBaRaBa: Sriramachandran *et al.* [90] provide measurements for 68 C $^4\Sigma^-$ –X $^4\Sigma^-$ transitions observed in sunspot spectra. These measurements are assigned based on the data of Lagerqvist and Selin [47], and as such also reported R- and P-branch transitions with 'a' and 'b' subscripts; their assignments were also updated to F_3 and F_2 fine structure components, respectively. 11 of these transitions, all in the (0,2) band, were been reported with the incorrect R-/P-branch labelling which was corrected.

09HoHaMa: Hopkins et al. [34] observed crucial spinforbidden intercombination transitions in the 2 $^2\Pi\text{--}X$ $^4\Sigma^-$ band system that connect the quartet components of our network to the doublets via the transitions involving the $2^{2}\Pi$ state reported by 87MeHuChTa [84]. The original spectra recorded by Hopkins et al. [34] was revisited and assigned as part of this work to ensure the key connection between spin components of the VO network was correct; this assignment process is discussed in detail below. Assignments for transitions involving the $2^{2}\Pi_{3/2}$, v = 0 state could be validated against the doublet data of 87MeHuChTa [84], whereas the $2^{2}\Pi_{1/2}$ bands had no other observations to compare against. This meant that while combination differences could be checked for the level energies of the 2 ${}^{2}\Pi_{3/2}$ state between sources, the 2 $^2\Pi_{1/2}$ state component could only be ensured to be self-consistent. In total, 191 transitions were assigned in these spectra. An unassigned 3 $^2\Pi$ -X $^4\Sigma$ - band system is also reported, though we make no attempt to assign these spectra as they do not connect to the rest of the doublet

As the doublet and quartet networks were only initially con-

nected through one spin-orbit component of the $2^{2}\Pi$ state, half of the doublet network was still unconnected. This was because all of the sources reporting doublet transitions exclusively observed P- and R-branch transitions, which for 87MeHuChTa [84] and 02RaBeDaMe [87] had $\Delta\Omega = \pm 1$ and for 05RaBe [88] $\Delta\Omega = 0$. This meant the 1 $^2\Delta_{3/2}$, 1 $^2\Pi_{1/2}$, 1 $^2\Phi_{5/2}$, 2 $^2\Delta_{3/2}$ and 3 ${}^{2}\Delta_{3/2}$ states were not connected to the quartet states via the newly assigned intercombination transitions observed by 09HoHaMa [34] and were split into two subgraphs based on their parity. We rectified this through the addition of calculated transition wavenumbers for both $Q_{21}(5.5)$ transitions in the $1^2\Delta - 1^2\Delta$ (0,0) band. These were derived from levels in the VOMYT line list, effectively estimating the spin-orbit splitting in the 1 $^2\Delta$ state which has not yet been observationally determined [87, 88]. These were entered as 356.596842 cm⁻¹ for the Q_{21ef} (5.5) transition and 356.596837 cm⁻¹ for Q_{21fe} (5.5). Both transitions are provided in the MARVEL input file with the source tag VOMYT_MAGIC. The 1 $^2\Delta$ state was chosen as it is both the lowest energy doublet state observed and the state involved in the most transitions within the doublet network. The value of J = 5.5 was chosen as it was the lowest value of J for which both total parity (+/-) levels in each spin-orbit component existed within the doublet data. This connection represents a weak point in the network and would benefit from observations involving the newly assigned $2^{2}\Pi_{1/2}$ state, such as the unobserved $2^{2}\Pi_{1/2}$ — $1^{2}\Delta_{3/2}$ band.

The perturbing state identified by 94ChHaHuHu [85] and 95AdBaBeBo [45] was originally reported as a $^2\Sigma^+$ but has been updated here to 1 $^2\Sigma^+$. This is to be consistent with the naming scheme for the other doublet electronic states, where each instance of the same electronic state configuration is numbered starting from the lowest energy.

3.2. New spectra assignment

Assignments of the spectra reported by 09HoHaMa [34] were carried out by first performing rough calculations to provide an initial estimate for the transitions frequencies. These estimates were produced for every expected set of P-, Q- and R-branch transitions in the observed bands and were generated using molecular constants published by 09HoHaMa [34]. These predictions were calculated using Eqs. (1) and (2) of 09HoHaMa [34], and were only dependent on the rotational constant B_v , the centrifugal distortion constant D_v , the spin-orbit coupling constant A_v and the Ω -doubling constant p_v and as such minor deviations from the predicted values were to be expected.

When assigning transitions in the $2^2\Pi_{1/2}$ – $X^4\Sigma^-$ (0,0) band, we were able to make assignments to at least one transition in 11 out of the 12 possible P-, Q- and R-branches. We were only unable to assign any transitions to the P₁₁ branch, due to our predictions showing the band to start around 18 048 cm⁻¹ and reflect back on itself at a band head at 18 050 cm⁻¹. Similarly, our predictions show the Q₁₂ branch forming a band head at around 18 046 cm⁻¹. In this case the branch reflects back on itself twice, explaining the extremely blended, high intensity feature observed on the lower energy side of the band origin. As such we were only able to confidently assign the first transition in this branch. These features can be seen in Fig. 3, along

with the rest of our final assignments to the 2 $^2\Pi_{1/2}$ –X $^4\Sigma^-$ (0,0) spectrum. With some coverage of almost all branches, we were able to assign 103 transitions in the 2 $^2\Pi_{1/2}$ –X $^4\Sigma^-$ (0,0) spectrum with individual transitions frequencies provided in Table 1.

Upon reanalysing the $2^{2}\Pi_{3/2}$ – $X^{4}\Sigma^{-}$ (0,0) data we were able to identify and assign some lines from the R₂₁, Q₂₁, R₂₂, P₂₂, P₂₃ and P₂₄ branches. The P₂₁ branch is predicted to fall near the heavily congested band origin and similarly the Q22 and R23 branches were both reflected at their band heads near the origin, significantly overlapping one another and making individual line assignments impossible. As such, further high-resolution study near the band origin would be needed to confidently assign these branches. The Q23, R24 and Q24 branches were additionally blended or too weak to assign. The transitions of the six assigned branches of the $2^{2}\Pi_{3/2}$ – $X^{4}\Sigma^{-}$ (0,0) system are shown in Fig. 4. Some branches rapidly became much weaker and were obscured by transitions from other branches, as can be seen with the P₂₃ branch and the more extensively assigned P₂₄ counterpart. As such, we were only able to assign 56 transitions for the $2^2\Pi_{3/2}$ $X^{4}\Sigma^{-}$ (0,0) spectrum; these are given in Table 1.

While assigning the $2^{2}\Pi_{3/2}$ – $X^{4}\Sigma^{-}$ (0,0) spectrum, we noticed a discrepancy in the R21 and P24 branches for lines between J'' = 7.5 - 11.5. For both branches, lines in this region appear at slightly higher wavenumbers than their predicted positions, shifted by up to ~ 0.75 cm⁻¹. This affect begins suddenly at J'' = 7.5, after which predictions start to close the gap on observed line centres, becoming consistent with actual observations again at J'' = 11.5. The R₂₁ branch can be assigned beyond this, where observed line centres begin to shift to slightly lower wavenumbers than their predicted values and are assigned up to J'' = 13.5. Above this point, transitions in these bands are too weak to assign. Comparing against calculated term energies for the lower, $X^{4}\Sigma^{-}$ state, these two branches displayed obs.—calc. residuals as a function of J'' that sharply increase at J'' = 7.5 before gradually returning to scatter about zero. It is likely that these transitions are perturbed by a nearby state, but we are unable to determine which.

The final spectrum we assigned was that of a $2^{2}\Pi_{1/2}$ – $X^{4}\Sigma^{-}$ (1,0) band. Here we made considerably fewer assignments than in the previous spectra as the majority of the branches we expected to be present and not locked up in band heads were too heavily blended to confidently make any assignments. As such, we have only made assignments to transitions in the R_{11} , Q_{11} and R₁₂ branches, all of which lie to the blue of the band origin where the spectrum is significantly less dense, as can be seen in Fig. 5. The 34 lines assigned to this band must be considered less reliable as they have fewer transitions to compare combination differences with or for the MARVEL procedure to evaluate their consistency against. While this higher vibrational band does not increase the connectivity between the quartet and doublet components of the network, it does provide information on the $2^{2}\Pi$ state vibrational excitation energy, which is useful for ab initio calculations.

The $2^{2}\Pi_{3/2}$ system took two attempts to assign in order to produce consistent data, whereas it only took a single attempt to assign a set of self-consistent transitions to both vibrational

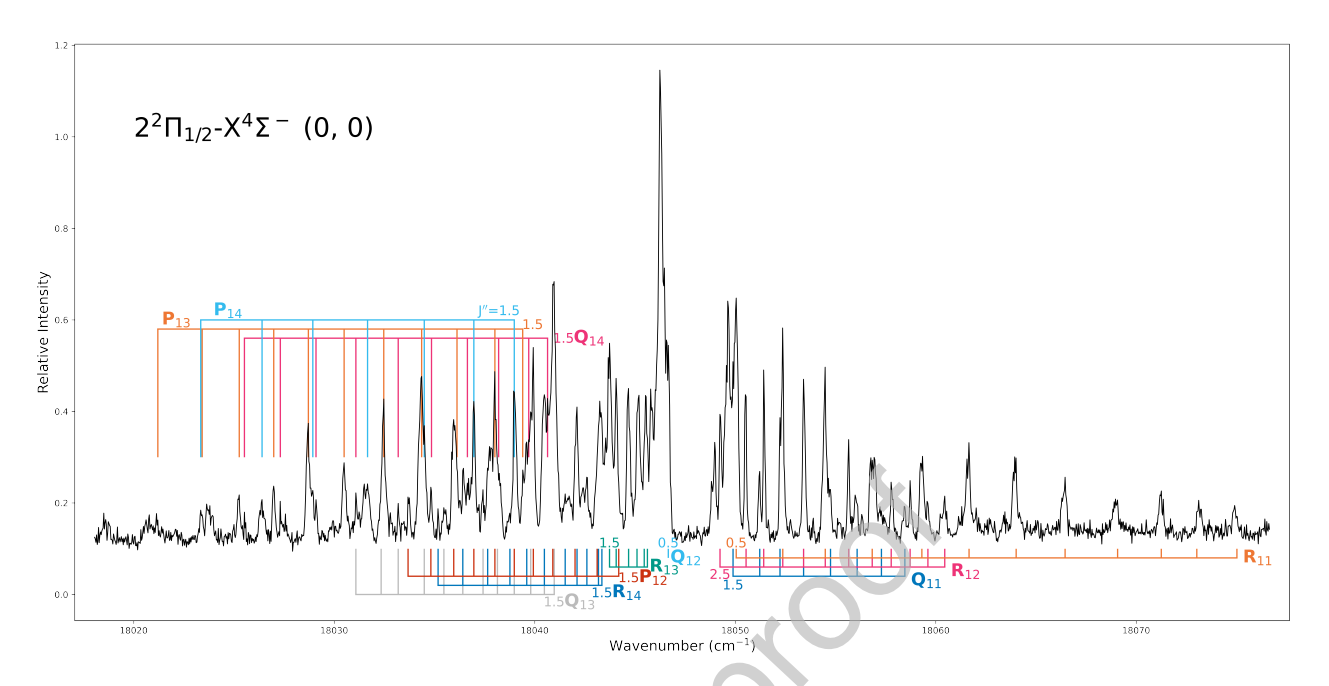


Fig. 3: The assigned branches of the $2^2\Pi_{1/2}$ –X $^4\Sigma^-$ (0,0) spectrum measured by Hopkins *et al.* [34]. Each branch is marked with the lowest value of J" in the series. Molecular constants fit to this spectra are given in Table 2.

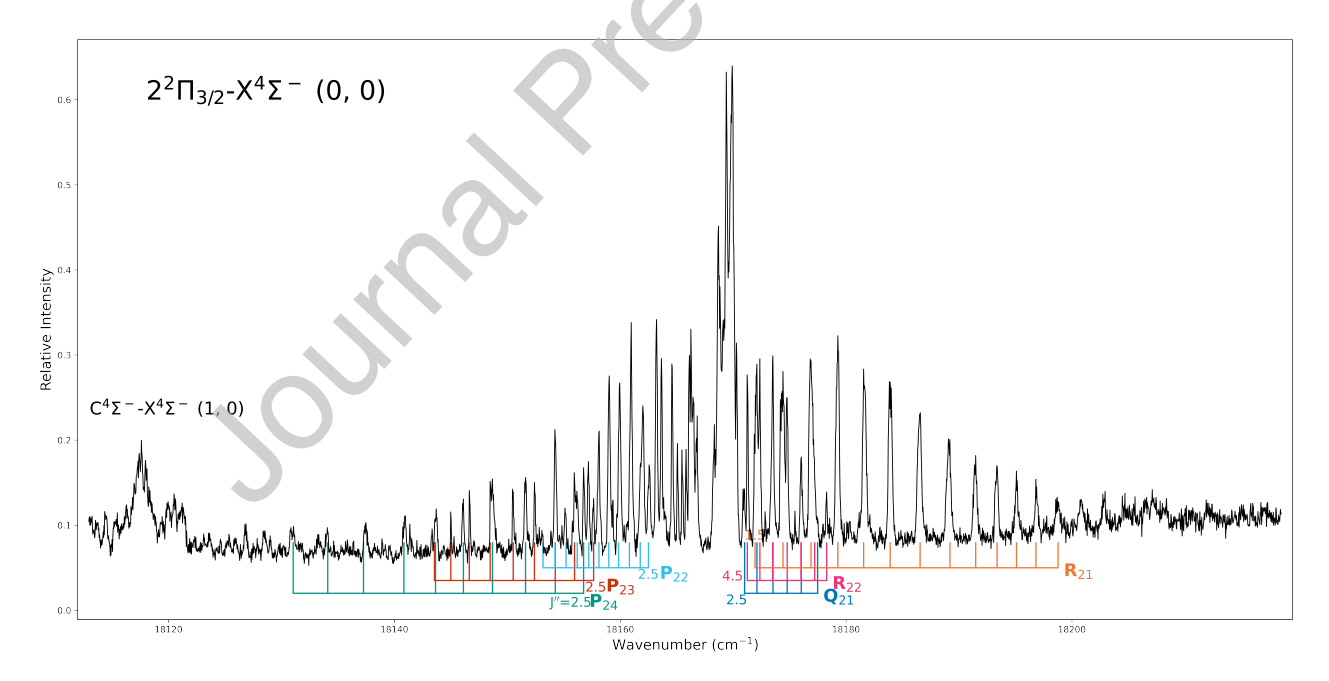


Fig. 4: The assigned branches of the $2\,^2\Pi_{3/2}$ – $X\,^4\Sigma^-$ (0,0) spectrum measured by Hopkins *et al.* [34]. Each branch is marked with the lowest value of J" in the series. Molecular constants fit to this spectra are given in Table 2. The unresolved profile of the $C\,^4\Sigma^-$ – $X\,^4\Sigma^-$ (1,0) band is marked on the left edge of the plot.

Fig. 5: The assigned branches of the $2^2\Pi_{1/2}$ -X $^4\Sigma^-$ (1,0) spectrum measured by Hopkins *et al.* [34]. Each branch is marked with the lowest value of J" in the series. Molecular constants fit to this spectra are given in Table 2. The unresolved profile of the C $^4\Sigma^-$ -X $^4\Sigma^-$ (2,0) band is marked on the plot.

Table 1: The assigned transitions of the $2^2\Pi - X^4\Sigma^-$ spectra reported in [34] and reanalysed in this work.

	$2^{2}\Pi_{1/2}$ -X $^{4}\Sigma^{-}(0,0)$										
$J^{\prime\prime}$	R_{11}	Q_{11}	R_{12}	Q_{12}	P_{12}	R_{13}	Q_{13}	P_{13}	R_{14}	Q_{14}	P ₁₄
0.5	18050.05			18046.66							
1.5	18052.37	18049.89			18044.19	18043.73	18040.97	18039.40	18043.35	18040.64	18038.98
2.5	18054.49	18051.22	18049.24		18043.11	18044.06	18040.48	18038.01	18043.18	18039.70	18036.96
3.5	18056.83	18052.23	18050.54		18042.01	18044.68	18039.80	18036.12	18042.60	18038.20	18034.49
4.5	18059.31	18053.41	18051.42		18040.90	18045.10	18038.98	18034.36	18042.11	18036.64	18031.66
5.5	18061.66	18054.75	18052.37		18039.93	18045.46	18038.14	18032.47	18041.52	18034.85	18028.93
6.5	18064.01	18056.08	18053.41		18038.98	18045.62	18037.42	18030.49	18040.48	18033.19	18026.40
7.5	18066.45	18057.29	18054.49		18038.01		18036.41	18028.71	18039.60	18031.08	18023.34
8.5	18069.07	18058.46	18055.66		18036.96		18035.47	18026.98	18038.76	18029.09	
9.5	18071.25		18056.83		18035.96		18034.49	18025.26	18037.65	18027.31	
10.5	18073.02		18057.78		18034.82		18033.19	18023.41	18036.41	18025.52	
11.5	18075.02		18058.72		18033.68		18032.34	18021.20	18035.18		
12.5			18059.61				18031.08				
13.5			18060.45								
			- 1	. 1					- 1 -		
			$2^{2}\Pi_{3/2}$ -X							$I_{1/2}$ – $X^{4}\Sigma^{-}$ (
$J^{\prime\prime}$	R ₂₁	Q_{21}	2 ² 11 _{3/2} –X R ₂₂	P_{22}	P ₂₃	P ₂₄		J''	R_{11}	$I_{1/2}$ – $X^{4}\Sigma^{-}$ (Q_{11}	(1,0) R ₁₂
0.5		Q ₂₁			P ₂₃	P ₂₄		0.5	R ₁₁ 18982.21		
0.5 1.5	18171.93			P ₂₂			, O	0.5 1.5	R ₁₁ 18982.21 18984.80	Q ₁₁	R ₁₂
0.5 1.5 2.5	18171.93 18174.41	18171.01		P ₂₂	18157.64	18156.75	(0)	0.5 1.5 2.5	R ₁₁ 18982.21 18984.80 18986.97	Q ₁₁ 18983.69	R ₁₂
0.5 1.5 2.5 3.5	18171.93 18174.41 18176.89	18171.01 18172.10	R ₂₂	P ₂₂ 18162.49 18161.77	18157.64 18155.95	18156.75 18154.24	10	0.5 1.5 2.5 3.5	R ₁₁ 18982.21 18984.80 18986.97 18989.28	Q ₁₁ 18983.69 18984.80	R ₁₂ 18981.60 18982.86
0.5 1.5 2.5 3.5 4.5	18171.93 18174.41 18176.89 18179.27	18171.01 18172.10 18173.52	R ₂₂	P ₂₂ 18162.49 18161.77 18160.81	18157.64 18155.95 18154.24	18156.75 18154.24 18151.61	0/0	0.5 1.5 2.5 3.5 4.5	R ₁₁ 18982.21 18984.80 18986.97 18989.28 18991.69	Q ₁₁ 18983.69 18984.80 18985.96	R ₁₂ 18981.60 18982.86 18983.80
0.5 1.5 2.5 3.5 4.5 5.5	18171.93 18174.41 18176.89 18179.27 18181.55	18171.01 18172.10 18173.52 18174.78	R ₂₂ 18171.25 18172.36	P ₂₂ 18162.49 18161.77 18160.81 18159.85	18157.64 18155.95 18154.24 18152.40	18156.75 18154.24 18151.61 18148.68	0,0	0.5 1.5 2.5 3.5 4.5 5.5	R ₁₁ 18982.21 18984.80 18986.97 18989.28 18991.69 18993.93	Q ₁₁ 18983.69 18984.80 18985.96 18987.11	R ₁₂ 18981.60 18982.86 18983.80 18984.80
0.5 1.5 2.5 3.5 4.5 5.5 6.5	18171.93 18174.41 18176.89 18179.27 18181.55 18183.90	18171.01 18172.10 18173.52 18174.78 18176.03	R ₂₂ 18171.25 18172.36 18173.49	P ₂₂ 18162.49 18161.77 18160.81 18159.85 18158.98	18157.64 18155.95 18154.24 18152.40 18150.52	18156.75 18154.24 18151.61 18148.68 18146.11	30	0.5 1.5 2.5 3.5 4.5 5.5 6.5	R ₁₁ 18982.21 18984.80 18986.97 18989.28 18991.69 18993.93 18996.09	Q ₁₁ 18983.69 18984.80 18985.96 18987.11 18988.34	R ₁₂ 18981.60 18982.86 18983.80 18984.80 18985.81
0.5 1.5 2.5 3.5 4.5 5.5 6.5 7.5	18171.93 18174.41 18176.89 18179.27 18181.55 18183.90 18186.55	18171.01 18172.10 18173.52 18174.78	R ₂₂ 18171.25 18172.36 18173.49 18174.78	P ₂₂ 18162.49 18161.77 18160.81 18159.85 18158.98 18158.11	18157.64 18155.95 18154.24 18152.40 18150.52 18148.77	18156.75 18154.24 18151.61 18148.68 18146.11 18143.64	300	0.5 1.5 2.5 3.5 4.5 5.5 6.5 7.5	R ₁₁ 18982.21 18984.80 18986.97 18989.28 18991.69 18993.93 18996.09 18998.12	Q ₁₁ 18983.69 18984.80 18985.96 18987.11 18988.34 18989.49	R ₁₂ 18981.60 18982.86 18983.80 18984.80 18985.81 18986.75
0.5 1.5 2.5 3.5 4.5 5.5 6.5 7.5 8.5	18171.93 18174.41 18176.89 18179.27 18181.55 18183.90 18186.55 18189.20	18171.01 18172.10 18173.52 18174.78 18176.03	R ₂₂ 18171.25 18172.36 18173.49 18174.78 18176.00	P ₂₂ 18162.49 18161.77 18160.81 18159.85 18158.98 18158.11 18157.21	18157.64 18155.95 18154.24 18152.40 18150.52 18148.77 18146.63	18156.75 18154.24 18151.61 18148.68 18146.11 18143.64 18140.84	(0)	0.5 1.5 2.5 3.5 4.5 5.5 6.5 7.5 8.5	R ₁₁ 18982.21 18984.80 18986.97 18989.28 18991.69 18993.93 18996.09 18998.12 19000.17	Q ₁₁ 18983.69 18984.80 18985.96 18987.11 18988.34 18989.49 18990.36	R ₁₂ 18981.60 18982.86 18983.80 18984.80 18985.81 18986.75 18987.72
0.5 1.5 2.5 3.5 4.5 5.5 6.5 7.5 8.5 9.5	18171.93 18174.41 18176.89 18179.27 18181.55 18183.90 18186.55 18189.20 18191.48	18171.01 18172.10 18173.52 18174.78 18176.03	R ₂₂ 18171.25 18172.36 18173.49 18174.78 18176.00 18177.22	P ₂₂ 18162.49 18161.77 18160.81 18159.85 18158.98 18158.11 18157.21 18156.19	18157.64 18155.95 18154.24 18152.40 18150.52 18148.77 18146.63 18144.99	18156.75 18154.24 18151.61 18148.68 18146.11 18143.64 18140.84 18137.26	(0)	0.5 1.5 2.5 3.5 4.5 5.5 6.5 7.5 8.5 9.5	R ₁₁ 18982.21 18984.80 18986.97 18989.28 18991.69 18993.93 18996.09 18998.12 19000.17 19002.19	Q ₁₁ 18983.69 18984.80 18985.96 18987.11 18988.34 18989.49	R ₁₂ 18981.60 18982.86 18983.80 18984.80 18985.81 18986.75 18987.72 18988.73
0.5 1.5 2.5 3.5 4.5 5.5 6.5 7.5 8.5 9.5 10.5	18171.93 18174.41 18176.89 18179.27 18181.55 18183.90 18186.55 18189.20 18191.48 18193.37	18171.01 18172.10 18173.52 18174.78 18176.03	R ₂₂ 18171.25 18172.36 18173.49 18174.78 18176.00	P ₂₂ 18162.49 18161.77 18160.81 18159.85 18158.98 18158.11 18157.21 18156.19 18155.20	18157.64 18155.95 18154.24 18152.40 18150.52 18148.77 18146.63	18156.75 18154.24 18151.61 18148.68 18146.11 18143.64 18140.84 18137.26 18134.09		0.5 1.5 2.5 3.5 4.5 5.5 6.5 7.5 8.5 9.5	R ₁₁ 18982.21 18984.80 18986.97 18989.28 18991.69 18993.93 18996.09 18998.12 19000.17 19002.19 19004.22	Q ₁₁ 18983.69 18984.80 18985.96 18987.11 18988.34 18989.49 18990.36	R ₁₂ 18981.60 18982.86 18983.80 18984.80 18985.81 18986.75 18987.72 18988.73 18989.67
0.5 1.5 2.5 3.5 4.5 5.5 6.5 7.5 8.5 9.5 10.5 11.5	18171.93 18174.41 18176.89 18179.27 18181.55 18183.90 18186.55 18189.20 18191.48 18193.37 18195.09	18171.01 18172.10 18173.52 18174.78 18176.03	R ₂₂ 18171.25 18172.36 18173.49 18174.78 18176.00 18177.22	P ₂₂ 18162.49 18161.77 18160.81 18159.85 18158.98 18158.11 18157.21 18156.19 18155.20 18154.21	18157.64 18155.95 18154.24 18152.40 18150.52 18148.77 18146.63 18144.99 18142.87	18156.75 18154.24 18151.61 18148.68 18146.11 18143.64 18140.84 18137.26		0.5 1.5 2.5 3.5 4.5 5.5 6.5 7.5 8.5 9.5 10.5	R ₁₁ 18982.21 18984.80 18986.97 18989.28 18991.69 18993.93 18996.09 18998.12 19000.17 19002.19 19004.22 19006.35	Q ₁₁ 18983.69 18984.80 18985.96 18987.11 18988.34 18989.49 18990.36	R ₁₂ 18981.60 18982.86 18983.80 18984.80 18985.81 18986.75 18987.72 18988.73 18989.67 18990.57
0.5 1.5 2.5 3.5 4.5 5.5 6.5 7.5 8.5 9.5 10.5	18171.93 18174.41 18176.89 18179.27 18181.55 18183.90 18186.55 18189.20 18191.48 18193.37	18171.01 18172.10 18173.52 18174.78 18176.03	R ₂₂ 18171.25 18172.36 18173.49 18174.78 18176.00 18177.22	P ₂₂ 18162.49 18161.77 18160.81 18159.85 18158.98 18158.11 18157.21 18156.19 18155.20	18157.64 18155.95 18154.24 18152.40 18150.52 18148.77 18146.63 18144.99 18142.87	18156.75 18154.24 18151.61 18148.68 18146.11 18143.64 18140.84 18137.26 18134.09		0.5 1.5 2.5 3.5 4.5 5.5 6.5 7.5 8.5 9.5	R ₁₁ 18982.21 18984.80 18986.97 18989.28 18991.69 18993.93 18996.09 18998.12 19000.17 19002.19 19004.22	Q ₁₁ 18983.69 18984.80 18985.96 18987.11 18988.34 18989.49 18990.36	R ₁₂ 18981.60 18982.86 18983.80 18984.80 18985.81 18986.75 18987.72 18988.73 18989.67

bands of the 2 $^2\Pi_{1/2}$ component. The majority of lines in these spectra are blended to some degree, especially lines to the red of the band origins; a conservative base uncertainty of $0.2~{\rm cm}^{-1}$ was used for all newly assigned transitions. Hence, though we could quote line positions to higher precision, we have chosen only to provide them to two decimal places. MARVEL and the method of combination differences were used to check the consistency of the final assignments by ensuring that the standard deviation of the energy of a given level was less than the uncertainty of the constituent transitions that defined that level.

Molecular constants were determined from effective Hamiltonian fits to the newly assigned spectra using program PGOPHER [46]. The fits were corroborated to ensure the empirical energies determined through MARVEL were reproduced to a reasonable accuracy. In the $2^2\Pi_{3/2}$, v=0 state, the constants also reproduce the higher-J levels known from the data of Merer *et al.* [84] well. These constants are tabulated in Table 2. The value of D_v was kept constant for the $2^2\Pi_{1/2}$ state with the value of 6×10^{-7} as attempts to float it yielded very high standard deviation results. This is likely because D_v scales with J^4 and

the spectra we were fitting went no higher than J=14.5 in the $2\,{}^2\Pi_{1/2},\,v=0,\,1$ states, leaving it very poorly determined. Additional observations to higher J would help to better constrain this constant. With the doublet network connected to the quartet ground state via the $2\,{}^2\Pi_{3/2}$ –X ${}^4\Sigma^-$ (0,0) data, we were able to determine T_v values for the other connected doublet states. The resulting values are consistent with the energy differences reported in the literature [84, 87, 88]. Values were also fit or the rotational constant B_v and the quartic centrifugal distortion constant D_v , while values for the sextic centrifugal distortion constant H_v and the Ω -doubling constants P_v and P_{D_v} were fit where possible.

It is noted in the literature [34, 43] that the levels of the $2\,^2\Pi$, v=n states are very close to those of C $^4\Sigma^-$, v=n+1; an example of this can be seen in the far left of Fig. 4 where the unresolved C $^4\Sigma^-$ –X $^4\Sigma^-$ (1,0) band approaches the edge of the $2\,^2\Pi_{3/2}$ –X $^4\Sigma^-$ (0,0) spectrum. Similarly, the unresolved C $^4\Sigma^-$ –X $^4\Sigma^-$ (2,0) band can be seen slightly closer to the $2\,^2\Pi_{1/2}$ –X $^4\Sigma^-$ (1,0) band centre in Fig. 5. This supports the theory that the $2\,^2\Pi$ state is responsible for the electronic perturbations observed in the C $^4\Sigma^-$ –X $^4\Sigma^-$ transitions included in our network [43, 47].

Table 2: Molecular constants (cm⁻¹) for the doublet states of VO contained with the MARVEL network, including the $2^{2}\Pi$ states observed in the newly assigned $2^{2}\Pi - X^{4}\Sigma^{-}$ spectra. Values provided in parentheses are the standard deviation in units of the last digit; entries without standard deviations were fixed in the fit.

State	υ	T_v	B_v	$10^{-7} \times D_v$	$10^{-11} \times H_v$	p_v	p_{D_v}
$1^{2}\Delta_{3/2}$	0	9681.1093(83)	0.550756(39)	6.17(45)	-2.9(14)		
$1^{2}\Delta_{3/2}$	1	10 673.994(11)	0.546 668(44)	7.19(44)	-8.1(13)		
$1^{2}\Delta_{5/2}$	0	10 037.7490(38)	0.551 989(22)	2.63(31)	-49.2(11)		
$1^{2}\Phi_{5/2}$	0	15 220.5620(59)	0.518 889(15)	5.707(73)			
$1^{2}\Phi_{7/2}$	0	15 589.4260(23)	0.520 562 2(72)	6.097(42)			
$1^{2}\Pi_{1/2}$	0	16 937.5312(67)	0.518 482(17)	5.934(80)		$1.424(10)\times10^{-2}$	-3.87×10^{-2a}
$1^{2}\Pi_{1/2}$	1	17 864.8170(66)	0.515 228(17)	6.122(82)		$1.543(10)\times10^{-2}$	-3.60×10^{-2a}
$1^{2}\Pi_{1/2}$	2	18 782.947(30)	0.511703(85)	5.34(47)		$1.81(10)\times10^{-2}$	$-3.00(84)\times10^{-6}$
$1^{2}\Pi_{1/2}$	3	19 691.204(12)	0.508 458(45)	6.91(34)		$1.683(17)\times10^{-2}$	
$1^{2}\Pi_{3/2}$	0	17 185.4577(26)	0.521 058 0(80)	6.452(45)		$-2.7(11)\times10^{-4}$	$4.20(91)\times10^{-7}$
$1^{2}\Pi_{3/2}$	1	18 112.4516(38)	0.518 019(18)	6.57(17)			
$2^{2}\Pi_{1/2}$	0	18 045.061(26)	0.521 31(27)	6.00^{b}		$2.61(21)\times10^{-5}$	
$2^{2}\Pi_{1/2}$	1	18 977.433(38)	0.51671(35)	6.00^{b}			
$2^{2}\Pi_{3/2}$	0	18 164.7228(63)	0.526 345(20)	5.58(12)			
$2^{2}\Delta_{3/2}$	0	24 856.5701(78)	0.487 822(22)	3.44(11)			
$2^{2}\Delta_{5/2}$	0	25 145.1608(33)	0.491 632(11)	6.441(70)			
$3^2\Delta_{3/2}$	0	31 718.896(11)	0.493 335(50)	5.67(55)	-3.2(17)		
$3^{2}\Delta_{5/2}$	0	32 012.5598(87)	0.495 472(94)	65.4(21)			

a: Values fixed to those provided in [88].

Unfortunately, our assignments of the $2^2\Pi - X^4\Sigma^-$ spectra do not extend to sufficiently high values of J to match those of the perturbed transitions, so we cannot explicitly confirm that this state is responsible.

4. MARVEL networks

We produced two final spectroscopic networks using the MARVEL procedure, one with resolved hyperfine structure and one without; these are presented below. Unlike in previous MARVEL studies, where the number of hyperfine-resolved transitions has been orders of magnitude less than that of hyperfine-unresolved transitions [51, 91–94], the VO data analysed in this work consisted of a much more even split (44.8% hyperfine-resolved data). As such, the MARVEL procedure yielded hyperfine-resolved and unresolved networks with a similar number of final energy levels. Hence, we chose to produce two distinct networks to preserve both data sets.

Many of the experimental sources considered in this work observed perturbations in their spectra, with many being able to be fully assigned. The perturbed transitions that have not been fully assigned are detailed in Table 3 and either consist of internal hyperfine perturbations observed below hyperfine resolution or perturbations by as yet unconfirmed electronic states.

4.1. Hyperfine-resolved network

To construct the hyperfine-resolved network, 6 643 transitions were passed through MARVEL for validation; 40 transitions were invalidated as they were found to be inconsistent with the rest of the network beyond their uncertainties. As expected,

the majority of the invalidated transitions are from the largest data source in this network, 82ChHaMe [43], accounting for half of the invalidated transitions. All of the data comprising this network is summarised in Table 4. The final hyperfineresolved network hence consists of 6 603 validated transitions, split between 139 components. The largest of these components comprises 6 452 transitions that determine 4 402 unique energy levels. Of the remaining components, the next largest consist of only 5 and then 4 transitions, followed by a further six components containing only 2 transitions. The remaining 130 components each consist of a single transition between two energy levels. This network connects hyperfine levels in the X $^4\Sigma^-$, B $^4\Pi$, C $^4\Sigma^-$ and 1 $^2\Sigma^+$ states.

4.2. Hyperfine-unresolved network

Validated transitions from the hyperfine-resolved network were deperturbed to yield equivalent hyperfine-unresolved transition frequencies, producing 946 deperturbed transitions. 99 and 77 O- and S-branch hyperfine transitions were excluded from the deperturbation process, due to the $|\Delta J| \leq 1$ constraint on the 6j-symbol in Eq. (1). All levels involved in the excluded transitions were also involved in at least one P-, Q- or R- branch transition, hence this did not reduce the total number of levels in the network. The deperturbed transitions were combined with the remaining 8 194 hyperfine-unresolved transitions, yielding 9 140 total transitions that were then passed through MARVEL for validation; these are summarised in Table 5. This final set of transitions comprises 8768 unique transitions; 372 transitions appear in two sources. All transitions from 81HoMeMi [83], 82ChHaMe [43], 91SuFrLoGi [56] and 08FlZi [44] contained within this network have been deperturbed, while the

b: Values kept fixed in the fit.

Table 3: A summary of the observed perturbations contained within the new networks presented in this work that have yet to be fully assigned.

Source	Band	Hyperfine Resolved	Number	Description
57LaSe [47]	$C^4\Sigma^ -X^4\Sigma^-$	No	28	Electronic perturbations to $C^4\Sigma^-$, $v' = 0, 1, 2$ at $N' =$
				73, 50, 25 respectively.
82ChHaMe [43]	C $^4\Sigma^-$ –X $^4\Sigma^-$	Yes	8	Unidentified electronic perturbation to $F_4(N' = 26)$.
		Yes	9	Unidentified electronic perturbation to $F_1(N' = 37)$.
82ChTaMe [82]	A $^4\Pi$ –X $^4\Sigma$ –	No	7	Internal hyperfine perturbation at $N'' = 15$.
87MeHuChTa [84]	D $^4\Delta$ –A' $^4\Phi$	No	2	Unidentified electronic perturbation to $F_1(N' = 28)$.

Table 4: The final hyperfine MARVEL network for VO, broken down by data source and vibronic band. The range in energy and total angular momentum quantum number J for transitions in each band is provided, along with their mean and maximum uncertainty. The total number of transitions validated compared to those accessed by MARVEL (V/A) is also given.

Band	Vib.	J range	V/A	Energy range (cm ⁻¹)	Unc. Mean/Max (cm ⁻¹)
81HoMeMi [83]					
C $^4\Sigma^-$ –X $^4\Sigma^-$	0 - 0	27.5 - 30.5	48/48	17336 - 17354	0.005/0.005
82ChHaMe [43]				X	
C $^4\Sigma^-$ –X $^4\Sigma^-$	0 - 0	0.5 - 47.5	2797/2817	17288 - 17427	0.002/0.005
91SuFrLoGi [56]					
$\mathrm{X}~^{4}\Sigma^{-}\mathrm{-X}~^{4}\Sigma^{-}$	0 - 0	0.5 - 1.5	3/3	0.2863 - 0.3664	$2.00 \times 10^{-7} / 2.00 \times 10^{-7}$
95AdBaBeBo [45	[]				
$1^{2}\Sigma^{+}$ – $X^{4}\Sigma^{-}$	2 - 0	37.5 - 40.5	14/14	12421 - 12432	0.002/0.002
B ${}^{4}\Pi_{-1/2}$ –X ${}^{4}\Sigma^{-}$	0 - 0	4.5 - 48.5	1027/1030	12408 - 12536	$7.61 \times 10^{-4} / 0.002$
$B^{4}\Pi_{1/2}-X^{4}\Sigma^{-}$	0 - 0	0.5 - 42.5	873/876	12490 - 12593	$8.16 \times 10^{-4} / 0.002$
$B^{4}\Pi_{3/2}-X^{4}\Sigma^{-}$	0 - 0	0.5 - 40.5	901/906	12491 - 12661	$9.50 \times 10^{-4} / 0.002$
$B^{4}\Pi_{5/2}-X^{4}\Sigma^{-}$	0 - 0	1.5 - 42.5	703/708	12575 - 12734	$8.86 \times 10^{-4} / 0.002$
08FlZi [44]			. (//	1	
X $^{4}\Sigma^{-}$ $ X$ $^{4}\Sigma^{-}$	0 - 0	6.5 - 17.5	220/224	9.7268 - 17.5154	$1.67 \times 10^{-6} / 1.67 \times 10^{-6}$

data of 95AdBaBeBo [45] is a mixture: 41.1% of the transitions accessed and 41.3% of those validated by MARVEL for this source are deperturbed. The deperturbed transitions involve 632 unique energy levels, 127 of which we were not present in any hyperfine-unresolved transition data.

53 of the input transitions were invalidated due to having optimal uncertainties determined by the MARVEL procedure significantly greater than their input uncertainty and being in poor agreement with their energies determined via combination differences. The largest number of invalidated transitions come from 87MeHuChTa [84], which is also the largest source of hyperfine-unresolved data. The final hyperfine-unresolved network hence contains 9 087 validated transitions divided into 121 components, the largest of which consists of 8 907 transitions that determine 4712 energy levels. Of the remaining components, six consist of 4 transitions, four consist of 3 transitions, a further 34 consist of 2 transitions and the remaining 76 are single-transitions components. A breakdown of the electronic states included in this network is shown in Fig. 6. The energy levels of the 2 ²Π state that are determined through our MARVEL analysis are shown in Fig. 7.

The exceptionally large maximum uncertainties in 82ChHaMe [43] and some bands of 95AdBaBeBo [45] seen in Table 5 are the result of our uncertainty scaling applied to a select few deperturbed hyperfine transitions, where the majority of the hyperfine components were absent from the data and those that were present were heavily skewed. Given the scaling factors defined

in Eq. (4) and Eq. (5), this has resulted in 8 and 12 transitions from the respective aforementioned sources with uncertainties above 1 cm⁻¹, all of which were validated by MARVEL.

The mean degree of the final energy levels determined by MARVEL, meaning the average number of transitions that define each level, is 3.78. 800 energy levels in the network are only defined by one transition and are hence unreliable. These levels primarily occur in the B $^4\Pi$ state (33.6%) followed by the A $^4\Pi$ (14.0%) and A' $^4\Phi$ (11.5%) states.

Using the empirical energies determined by MARVEL, it is possible to determine a larger set of possible transition frequencies. 119 203 allowed transitions can be determined between the 4712 unique energy levels, excluding any intercombination bands not reported in observations and ignoring unassigned perturbations, 110 435 of which are transitions not contained within the observational data.

By uniting the doublet and quartet states into a single network we were able to constrain the T_v values for the doublet states. These had previously been undetermined relative to the ground state [84, 87, 88]. These values are provided in Table 2.

Comparisons can be made between the empirical hyperfine-unresolved energies determined in this work and those calculated by McKemmish et~al.~ [30] as part of the VOMYT line list. Matching levels exactly using the MARVEL quantum numbers, $4\,350$ levels are identified in both the MARVEL and VOMYT lists. This matching set of levels primarily excludes the $2\,^2\Delta$ and $3\,^2\Delta$ electronic states, which were not considered in the original

Table 5: The final hyperfine-unresolved Marvel network for VO, broken down by data source and vibronic band. The range in energy and total angular momentum quantum number J for transitions in each band is provided, along with their mean and maximum uncertainty. The total number of transitions validated compared to those accessed by Marvel (V/A) is also given.

Band	Vib.	J range	V/A	Energy range (cm ⁻¹)	Unc. Mean/Max (cm ⁻¹)
57LaSe [47]	V10.	J runge	*//1	Energy range (cm)	one: wiedinwiak (em)
$C^{4}\Sigma^{-}-X^{4}\Sigma^{-}$	0 - 0	12.5 - 85.5	265/265	17026 - 17423	0.055/0.100
$C^{4}\Sigma^{-}-X^{4}\Sigma^{-}$	0 - 1	11.5 - 85.5	267/267	16028 - 16422	0.050/0.050
$C^{4}\Sigma^{-}-X^{4}\Sigma^{-}$	0 - 2	11.5 - 68.5	168/168	15284 - 15431	0.071/0.100
$C^{4}\Sigma^{-}-X^{4}\Sigma^{-}$	1 - 0	12.5 - 87.5	258/258	17868 - 18275	0.051/0.100
$C^{4}\Sigma^{-}-X^{4}\Sigma^{-}$	2 - 0	14.5 - 72.5	180/180	18771 - 19116	0.058/0.100
81HoMeMi [83]	2-0	14.5 - 72.5	100/100	10//1 - 19110	0.038/0.100
$C^{4}\Sigma^{-}-X^{4}\Sigma^{-}$	0 - 0	27.5 - 30.5	6/6	17336 - 17354	0.027/0.027
82ChHaMe [43]	0 - 0	21.5 - 50.5	0/0	17330 - 17334	0.027/0.027
$C^{4}\Sigma^{-}-X^{4}\Sigma^{-}$	0 - 0	0.5 - 47.5	367/367	17288 - 17427	0.100/4.875
82ChTaMe [82]	0 - 0	0.5 - 47.5	3011301	17200 - 17427	0.100/4.073
A ${}^{4}\Pi_{-1/2}$ – X ${}^{4}\Sigma^{-}$	0 - 0	4.5 - 89.5	197/197	9258 - 9481	0.007/0.010
$A^{4}\Pi_{-1/2} - X^{4}\Sigma^{-1}$	0 - 1	8.5 - 67.5	114/114	8364 - 8481	0.007/0.010
$A H_{-1/2} - X Z$ $A H_{-1/2} - X Y$	0 - 0	14.5 - 78.5	153/155	9312 - 9493	0.006/0.010
		20.5 - 66.5			
$A^{4}\Pi_{1/2} - X^{4}\Sigma^{-}$	0 - 1		69/69	8374 - 8476 9290 - 9538	0.006/0.010
$A^{4}\Pi_{3/2} - X^{4}\Sigma^{-}$	0 - 0	13.5 - 74.5	166/170		0.006/0.010
$A^{4}\Pi_{3/2} - X^{4}\Sigma^{-}$	0 - 1	9.5 - 54.5	71/72	8419 - 8514	0.006/0.010
$A^{4}\Pi_{5/2} - X^{4}\Sigma^{-}$	0 - 0	3.5 - 89.5	219/221	9262 - 9558	0.007/0.010
A ${}^{4}\Pi_{5/2}$ – X ${}^{4}\Sigma^{-}$	0 - 1	7.5 - 33.5	53/53	8521 - 8558	0.007/0.010
87MeHuChTa [84]	0 0	5 5 47 5	211/211	7160 7066	0.006/0.020
$1^{2}\Pi_{1/2}-1^{2}\Delta_{3/2}$	0 - 0	5.5 - 47.5	211/211	7160 - 7266	0.006/0.020
$1^{2}\Pi_{1/2}-1^{2}\Delta_{3/2}$	1 - 0	4.5 - 46.5	217/217	8057 - 8192	0.015/0.200
$1 {}^{2}\Pi_{1/2} - 1 {}^{2}\Delta_{3/2}$	2 - 1	4.5 - 42.5	163/163	8031 - 8117	0.017/0.200
$1 {}^{2}\Pi_{1/2} - 1 {}^{2}\Delta_{3/2}$	3 - 1	6.5 - 35.5	103/103	8962 - 9025	0.022/0.200
$1 {}^{2}\Pi_{3/2} - 1 {}^{2}\Delta_{5/2}$	0 - 0	4.5 - 46.5	208/208	7048 - 7157	0.006/0.020
$1 {}^{2}\Pi_{3/2} - 1 {}^{2}\Delta_{5/2}$	1 - 0	3.5 - 33.5	140/140	8008 - 8083	0.008/0.020
$2^{2}\Delta_{3/2}-1^{2}\Phi_{5/2}$	0 - 0	2.5 - 44.5	168/184	9568 - 9644	0.016/0.200
$2^{2}\Delta_{5/2}-1^{2}\Phi_{7/2}$	0 - 0	2.5 - 40.5	162/162	9483 - 9565	0.023/0.200
$2 {}^{2}\Pi_{3/2} - 1 {}^{2}\Delta_{5/2}$	0-0	3.5 - 42.5	162/162	8063 - 8138	0.020/0.200
$D^{4}\Delta_{1/2}-A^{4}\Pi_{-1/2}$	0 - 0	4.5 - 27.5	37/37	9526 - 9557	0.020/0.200
$D^{4}\Delta_{3/2}-A^{4}\Pi_{1/2}$	0 - 0		153/153	9567 - 9632	0.019/0.200
$D^{4}\Delta_{5/2}$ $-A^{4}\Pi_{3/2}$	0 - 0	3.5 - 29.5	63/66	9647 - 9688	0.020/0.200
$D^{4}\Delta_{7/2}$ $-A^{4}\Pi_{5/2}$	0 - 0	4.5 - 30.5	115/116	9690 - 9740	0.011/0.200
$D^{4}\Delta_{1/2}$ $-A'^{4}\Phi_{3/2}$	0 - 0	2.5 - 40.5	192/192	11946 - 12016	0.014/0.200
$D^{4}\Delta_{1/2}$ $-A'^{4}\Phi_{3/2}$	0 - 1	4.5 - 28.5	70/70	11033 - 11067	0.005/0.005
${ m D}^{4}\Delta_{1/2}$ ${ m -A'}^{4}\Phi_{3/2}$	1 - 0	4.5 - 28.5	96/96	12793 - 12833	0.007/0.020
$D^{4}\Delta_{3/2}$ $-A'^{4}\Phi_{5/2}$	0 - 0	7.5 - 41.5	107/107	11867 - 11928	0.011/0.200
$D^{4}\Delta_{3/2}$ $-A'^{4}\Phi_{5/2}$	0 - 1	10.5 - 20.5	38/38	10961 - 10987	0.005/0.005
$D^{4}\Delta_{3/2}$ $-A'^{4}\Phi_{5/2}$	1 - 0	4.5 - 27.5	73/73	12715 - 12764	0.006/0.020
$D^{4}\Delta_{5/2}$ $-A'^{4}\Phi_{7/2}$	0 - 0	7.5 - 51.5	242/242	11713 - 11863	0.009/0.200
$D^{4}\Delta_{5/2}$ $-A'^{4}\Phi_{7/2}$	0 - 1	9.5 - 48.5	204/204	10811 - 10929	0.010/0.200
$D^{4}\Delta_{5/2}$ $-A'^{4}\Phi_{7/2}$	1 - 0	13.5 - 36.5	78/78	12630 - 12685	0.018/0.200
$D^{4}\Delta_{5/2}-A'^{4}\Phi_{7/2}$	1 - 2	13.5 - 42.5	168/168	10730 - 10836	0.008/0.020
$D^{4}\Delta_{7/2}$ $-A'^{4}\Phi_{9/2}$	0 - 0	12.5 - 47.5	164/164	11710 - 11795	0.009/0.200
$D^{4}\Delta_{7/2}$ $-A'^{4}\Phi_{9/2}$	0 - 1	18.5 - 43.5	82/82	10787 - 10848	0.007/0.020
$D^{4}\Delta_{7/2}$ $-A'^{4}\Phi_{9/2}$	1 - 0	14.5 - 39.5	98/98	12529 - 12617	0.021/0.200
$D^{4}\Delta_{7/2}$ $-A'^{4}\Phi_{9/2}$	1 - 2	17.5 - 42.5	110/110	10677 - 10768	0.006/0.020
91SuFrLoGi [56]					
$X^{4}\Sigma^{-}$ $-X^{4}\Sigma^{-}$	0 - 0	0.5 - 1.5	1/1	0.3042 - 0.3042	$5.95 \times 10^{-6} / 5.95 \times 10^{-6}$

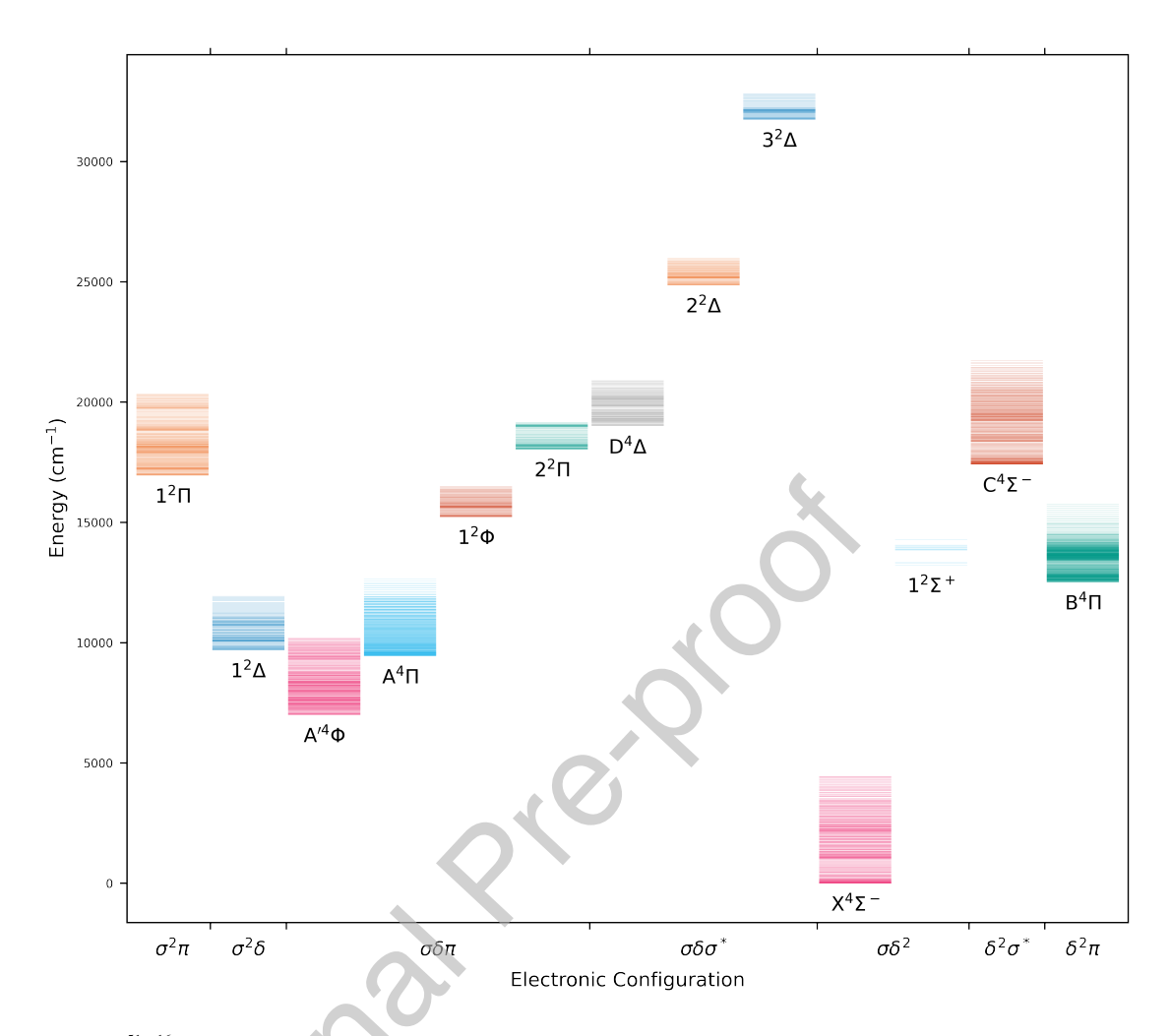


Fig. 6: The levels of $^{51}V^{16}O$ in our new network, grouped by electronic state and ordered by increasing T_0 values for each electron configuration. Each horizontal line represents an energy level in that electronic state.

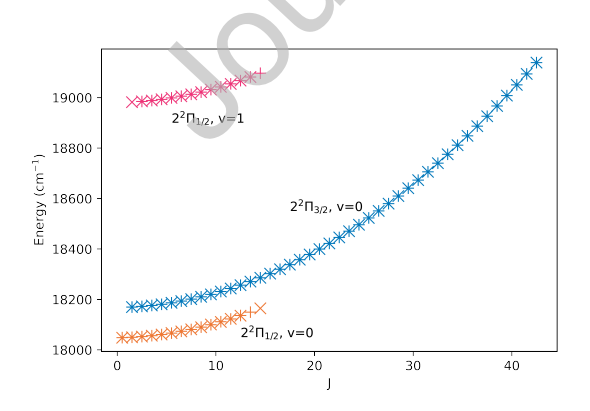


Fig. 7: The energy levels of the $2^2\Pi$ system determined by MARVEL as part of the hyperfine-unresolved network. Levels are marked with a '+' or 'x' based on their +/- total parity assignment, respectively.

VOMYT model, as well as any of the not yet fully assigned perturbations remaining within the MARVEL network. Minor adjustments were made to the quantum number assignment that had been provided by DUO for the levels of the VOMYT line list as, although the assignment of J and parity are rigorous, the labelling of other quantum numbers is not. In the vast majority of cases the assignment of these quantum numbers is performed correctly. However, for several pairs of levels with similar energies that differed only in their Ω assignment we identified through comparison with the empirical MARVEL energies that their Ω assignments had been swapped. Upon correcting this, we were able to measure how well the VOMYT model predicted the marvelised data: the $X\,^4\Sigma^-$ state was the best modelled with a mean obs. - calc. value of -0.0141 cm⁻¹. This difference is at least an order of magnitude larger for the other electronic states and is largest for A' $^4\Phi$ (-2.92 cm $^{-1}$) in the quartets and $1\,^2\Sigma^+$ (-8.20 cm $^{-1}$) in the doublets. These comparisons are summarised in Table 6 where obs. - calc. values are given for the

Table 5 - continued

Band	Vib.	J range	V/A	Energy range (cm ⁻¹)	Unc. Mean/Max (cm ⁻¹)
94ChHaHuHu [8:				. 6, . 6 ()	
$1^{2}\Sigma^{+}-X^{4}\Sigma^{-}$	3 - 0	27.5 - 33.5	7/7	13400 - 13413	0.020/0.020
B ${}^{4}\Pi_{-1/2}$ –X ${}^{4}\Sigma^{-}$	1 - 0	3.5 - 40.5	108/112	13354 - 13409	0.007/0.020
B ${}^{4}\Pi_{1/2}$ –X ${}^{4}\Sigma^{-}$	1 - 0	5.5 - 38.5	92/96	13360 - 13476	0.006/0.020
$B^{4}\Pi_{3/2}-X^{4}\Sigma^{-}$	1 - 0	5.5 - 42.5	93/97	13486 - 13556	0.005/0.020
${ m B}{}^4\Pi_{5/2}{-}{ m X}{}^4\Sigma^-$	1 - 0	3.5 - 41.5	154/159	13534 - 13631	0.005/0.020
95AdBaBeBo [45	5]				
$1^{2}\Sigma^{+}$ $-X^{4}\Sigma^{-}$	2 - 0	37.5 - 57.5	12/12	12421 - 12436	0.338/2.250
B $^4\Pi_{-1/2}$ –X $^4\Sigma^-$	0 - 0	1.5 - 61.5	382/383	12368 - 12536	0.064/2.250
${ m B}{}^4\Pi_{1/2}{-}{ m X}{}^4\Sigma^-$	0 - 0	0.5 - 92.5	315/316	12213 - 12593	0.048/2.250
B ${}^{4}\Pi_{3/2}$ –X ${}^{4}\Sigma^{-}$	0 - 0	0.5 - 53.5	257/258	12491 - 12661	0.030/0.562
B ${}^{4}\Pi_{5/2}$ –X ${}^{4}\Sigma^{-}$	0 - 0	1.5 - 49.5	323/326	12575 - 12734	0.051/2.250
97KaLiLuSa [86]					
A $^4\Pi_{-1/2}$ –X $^4\Sigma^-$	0 - 0	0.5 - 4.5	10/10	9453 - 9460	0.050/0.050
A $^4\Pi_{1/2}$ –X $^4\Sigma^-$	0 - 0	0.5 - 6.5	20/20	9481 - 9498	0.050/0.050
A $^4\Pi_{3/2}$ –X $^4\Sigma^-$	0 - 0	0.5 - 5.5	10/10	9516 - 9528	0.050/0.050
A $^4\Pi_{5/2}$ –X $^4\Sigma^-$	0 - 0	1.5 - 5.5	7/7	9559 - 9568	0.050/0.050
02RaBeDaMe [87	-				
$1^{2}\Phi_{5/2}-1^{2}\Delta_{3/2}$	0 - 0	6.5 - 47.5	224/224	5433 - 5548	0.003/0.003
$1 {}^{2}\Phi_{7/2} - 1 {}^{2}\Delta_{5/2}$	0 - 0	2.5 - 41.5	212/212	5462 - 5561	0.003/0.003
05RaBe [88]					
$3^{2}\Delta_{3/2}-1^{2}\Delta_{3/2}$	0 - 0	7.5 - 46.5	136/136	21866 - 22042	0.005/0.005
$3^{2}\Delta_{3/2}-1^{2}\Delta_{3/2}$	0 - 1	4.5 - 47.5	146/146	20877 - 21050	0.005/0.005
$3^{2}\Delta_{5/2}-1^{2}\Delta_{5/2}$	0 - 0	6.5 - 19.5	50/50	21932 - 21980	0.005/0.005
08FlZi [44]					5 5
$X {}^4\Sigma^ X {}^4\Sigma^-$	0 - 0	6.5 - 17.5	28/28	9.7287 - 17.5151	$1.05 \times 10^{-5} / 1.95 \times 10^{-5}$
08SrBaRaBa [90]					
$C^{4}\Sigma^{-}-X^{4}\Sigma^{-}$	0 - 2	14.5 - 67.5	16/16	15289 - 15431	0.050/0.050
$C^{4}\Sigma^{-}-X^{4}\Sigma^{-}$	1 - 0	14.5 - 74.5	26/26	17971 - 18270	0.050/0.050
$C^4\Sigma^ -X^4\Sigma^-$	2 - 0	14.5 - 67.5	25/26	18771 - 19116	0.050/0.050
09HoHaMa [34]	0.0		101401	10001 10007	0.0000.000
$2^{2}\Pi_{1/2}-X^{4}\Sigma^{-}$	0 - 0		101/101	18021 - 18075	0.200/0.200
$2^{2}\Pi_{1/2}-X^{4}\Sigma^{-}$	1 - 0	0.5 - 14.5	33/33	18982 - 19010	0.200/0.200
$2^{2}\Pi_{3/2}$ -X $^{4}\Sigma^{-}$	0 - 0	1.5 - 14.5	56/56	18131 - 18199	0.200/0.200
VOMYT_MAGIC			2/2	257 257	0.100/0.100
$1^{2}\Delta_{5/2}-1^{2}\Delta_{3/2}$	0 - 0	5.5 - 5.5	2/2	357 - 357	0.100/0.100

full set of data and for only levels where v = 0. This is because the potential curves used in the VOMYT spectroscopic model primarily relied on v = 0 data and as such it is perhaps more insightful to see how well the model predicts these energies.

5. Conclusion

We have performed a Marvel analysis for vanadium oxide constructing two networks, one hyperfine-resolved and one not, which are roughly equally sized. Comparison with the energy levels provide by the VOMYT line list suggest ways that the underlying spectroscopic model for VO can be improved. However, the hyperfine splitting in VO spectra, particularly those involving the X $^4\Sigma^-$ ground state, is sufficiently large that provision of a high accuracy line list for VO will require a treatment

of hyperfine interactions. Recently Qu *et al.* [89] have implemented a full (i.e. non-perturbative) treatment of hyperfine interactions within the Duo nuclear motion code. Our intention is to use this code and the energy levels here presented here to build an improved, hyperfine-resolved spectroscopic model for VO which will form the basis for a new line list.

While there is considerable experimental data available for VO which we have been able to use, and indeed validate, in this study, there are some notable gaps. Probably the most serious is the lack of any hyperfine-resolved observations involving vibrationally excites state of the electronic ground state which would allow the hyperfine structure as function of v to be characterized. Observations to connect the components of the doublet network without the use of calculated transition frequencies, such as the $2\,^2\Pi_{1/2}$ – $1\,^2\Delta_{3/2}$ band, would provide insight into the magnitude of the doublet states' spin-orbit separations. Assignments to the

Table 6: The obs. – calc. comparisons between the energies of the hyperfine-unresolved network and the VOMYT line list [30]. The mean obs. – calc. value and its standard deviation are provided for each electronic state for all available data, as well as only for data where v = 0.

	All Data obs.	. – calc. (cm ⁻¹)	v = 0 obs. – calc. (cm ⁻¹)		
Electronic State	Mean	Std. Dev.	Mean	Std. Dev.	
$X^4\Sigma^-$	-0.014106	0.290408	0.098649	0.105588	
A' 4Φ	-2.916455	4.842853	-4.146597	5.451342	
$\mathrm{A}^4\Pi$	0.275672	4.369407	0.275672	4.369407	
$\mathrm{B}~^4\Pi$	-1.790521	19.443214	-2.689856	24.393345	
$\mathrm{C}~^4\Sigma^-$	1.802196	3.367137	0.243359	0.401965	
$\mathrm{D}\ ^4\Delta$	-0.904808	4.983605	-0.202608	0.333345	
$1^{2}\Delta$	0.638876	0.645049	0.786097	0.287719	
$1^2\Sigma^+$	-8.198526	15.451711			
$1^{2}\Phi$	0.697798	0.490123	0.697798	0.490123	
$1^{2}\Pi$	1.251512	0.618625	0.876099	0.638034	
$2~^2\Pi$	3.611791	5.191570	4.524782	5.366077	

observed 3 $^2\Pi$ -X $^4\Sigma^-$ bands [34] would enable the extension of the network to additional electronic states, though would not increase the connectivity between the quartets and the rest of the doublet states. These and other experimental measurements would be welcome. As marvel is an active process, the networks presented here will continue to be updated with new and assigned spectroscopic data when it is made available.

Though hyperfine-resolved data remains limited in its electronic state and vibrational band coverage, the data that does exist consists of the most accurate transition measurements currently available. As such, a treatment of hyperfine-resolved data is necessary to achieve a high-resolution network and in turn, line list. Given that future experimental observations of the spectra of VO are likely to continue to be a mix of hyperfine resolved and hyperfine unresolved, hyperfine deperturbation techniques such as those employed here will remain a necessary step in MARVEL analysis.

Acknowledgements

We thank Tibor Furtenbacher for providing a version of MARVEL3, and him and Laura McKemmish for helpful conversations. This work was funded by the European Research Council (ERC) under the European Union's Horizon 2020 research and innovation programme through Advance Grant number 883830 and STFC through grant ST/R000476/1.

Data Availability

The Marvel transitions and energy files are given as supplementary material. The 191 newly assigned transitions of the $2\,^2\Pi$ -X $^4\Sigma^-$ band system are included in the Marvel transitions file, each marked with the source tag 09HoHaMa and a counting number.

- P. C. Keenan, L. W. Schroeder, An infrared system of bands of VO in M-type stars, Astrophys. J. 115 (1952) 82–88. doi:10.1086/145515.
- [2] H. Spinrad, R. F. Wing, Infrared spectra of stars, Ann. Rev. Astron. Astrophys 7 (1969) 249. doi:10.1146/annurev.aa.07.090169.001341.

- [3] J. D. Kirkpatrick, T. J. Henry, D. W. McCarthy, Jr., A standard stellar spectral sequence in the red/near-infrared - Classes K5 to M9, Astrophys. J. Suppl. 77 (1991) 417–440. doi:10.1086/191611.
- [4] J. D. Kirkpatrick, D. M. Kelly, G. H. Rieke, J. Liebert, F. Allard, R. Wehrse, M dwarf spectra from 0.6 to 1.5 micron-A spectral sequence, model atmosphere fitting, and the temperature scale, Astrophys. J. 402 (1993) 643–654. doi:10.1086/172166.
- [5] F. Allard, P. H. Hauschildt, Model atmospheres for M (sub)dwarf stars. 1: The base model grid, Astrophys. J. 445 (1995) 433–450. doi:10.1086/ 175708
- [6] J. D. Kirkpatrick, T. J. Henry, D. A. Simons, The solar neighborhood. 2: The first list of dwarfs with spectral types of M7 and cooler, Astron. J. 109 (1995) 797–807. doi:10.1086/117323.
- [7] A. Lançon, P. H. Hauschildt, D. Ladjal, M. Mouhcine, Near-IR spectra of red supergiants and giants, Astron. Astrophys. 468 (2007) 205–220. doi:10.1051/0004-6361:20065824.
- [8] C. M. Sharp, A. Burrows, Atomic and molecular opacities for brown dwarf and giant planet atmospheres, Astrophys. J. Suppl. 168 (2007) 140–166. doi:10.1086/508708.
- [9] P. F. Bernath, Molecular astronomy of cool stars and sub-stellar objects, Int. Rev. Phys. Chem. 28 (2009) 681–709. doi:10.1080/01442350903292442.
- [10] A.-S. Rajpurohit, C. Reylé, M. Schultheis, F. Allard, R. Scholz, D. Homeier, Stellar parameters of M dwarfs from low and high-resolution spectra together with new model atmospheres, in: S. Boissier, P. de Laverny, N. Nardetto, R. Samadi, D. Valls-Gabaud, H. Wozniak (Eds.), SF2A-2012: Proceedings of the Annual meeting of the French Society of Astronomy and Astrophysics, 2012, pp. 383–388.
- [11] A. S. Rajpurohit, C. Reylé, F. Allard, R. D. Scholz, D. Homeier, M. Schultheis, A. Bayo, High-resolution spectroscopic atlas of M subdwarfs. Effective temperature and metallicity, Astron. Astrophys. 564 (2014) A90. doi:10.1051/0004-6361/201322881.
- [12] J. D. Kirkpatrick, T. J. Henry, J. Liebert, The unique spectrum of the brown dwarf candidate GD 165B and comparison to the spectra of other lowluminosity objects, Astrophys. J. 406 (1993) 701–707. doi:10.1086/ 172480.
- [13] M. C. Cushing, J. T. Rayner, W. D. Vacca, An Infrared Spectroscopic Sequence of M, L, and T Dwarfs, Astrophys. J. 623 (2005) 1115. doi: 10.1086/428040.
- [14] H. Spinrad, R. L. Younkin, Infrared Bands of Vanadium Oxide in Three Mira Stars, Publ. Astron. Soc. Pac. 78 (1966) 65–67.
- [15] R. F. Wing, H. Spinrad, L. V. Kuhi, Infrared Stars, Astrophys. J. 147 (1967) 117.
- [16] M. W. Castelaz, D. G. Luttermoser, R. A. Piontek, Vanadium oxide in the spectra of Mira variables, Astrophys. J. 538 (2000) 341–345. doi: 10.1086/309121.
- [17] R. Tylenda, T. Kamiński, M. Schmidt, R. Kurtev, T. Tomov, Highresolution optical spectroscopy of V838 Monocerotis in 2009, Astron. Astrophys. 532 (2011) A138. doi:10.1051/0004-6361/201116858.

- [18] T. Kamiński, M. Schmidt, R. Tylenda, V4332 Sagittarii: a circumstellar disc obscuring the main object, Astron. Astrophys. 522 (2010) A75. doi: 10.1051/0004-6361/201014406.
- [19] J. J. Fortney, K. Lodders, M. S. Marley, R. S. Freedman, A Unified Theory for the Atmospheres of the Hot and Very Hot Jupiters: Two Classes of Irradiated Atmospheres, Astrophys. J. 678 (2008) 1419–1435. doi:10.1086/528370.
- [20] A. P. Showman, J. J. Fortney, Y. Lian, M. S. Marley, R. S. Freedman, H. A. Knutson, D. Charbonneau, Atmospheric circulation of hot Jupiters: coupled radiative-dynamical general circulation model simulations of HD 189733b and HD 209458b, Astrophys. J. 699 (2009) 564–584. doi: 10.1088/0004-637x/699/1/564.
- [21] M. Agúndez, V. Parmentier, O. Venot, F. Hersant, F. Selsis, Pseudo 2D chemical model of hot-Jupiter atmospheres: application to HD 209458b and HD 189733b, Astron. Astrophys. 564 (2014) A73. doi:10.1051/0004-6361/201322895.
- [22] K. Haynes, A. M. Mandell, N. Madhusudhan, D. Deming, H. Knut-son, Spectroscopic Evidence for a Temperature Inversion in the Dayside Atmosphere of Hot Jupiter WASP-33b, Astrophys. J. 806 (2015) 146. doi:10.1088/0004-637X/806/2/146.
- [23] Q. Changeat, B. Edwards, A. F. Al-Refaie, A. Tsiaras, J. W. Skinner, J. Y. K. Cho, K. H. Yip, L. Anisman, M. Ikoma, M. F. Bieger, O. Venot, S. Shibata, I. P. Waldmann, G. Tinetti, Five key exoplanet questions answered via the analysis of 25 hot-jupiter atmospheres in eclipse, Astrophys. J. Suppl. 260 (2022) 3. doi:10.3847/1538-4365/ac5cc2.
- [24] T. M. Evans, D. K. Sing, H. R. Wakeford, N. Nikolov, G. E. Ballester, B. Drummond, T. Kataria, N. P. Gibson, D. S. Amundsen, J. Spake, Detection of H₂O and evidence for tio/vo in an ultra-hot exoplanet atmosphere, Astrophys. J. 822 (2016) L4. doi:10.3847/2041-8205/822/1/14.
- [25] T. M. Evans, D. K. Sing, T. Kataria, J. Goyal, N. Nikolov, H. R. Wakeford, D. Deming, M. S. Marley, D. S. Amundsen, G. E. Ballester, J. K. Barstow, L. Ben-Jaffel, V. Bourrier, L. A. Buchhave, O. Cohen, D. Ehrenreich, A. G. Muñoz, G. W. Henry, H. Knutson, P. Lavvas, A. L. des Etangs, N. K. Lewis, M. López-Morales, A. M. Mandell, J. Sanz-Forcada, P. Tremblin, R. Lupu, An ultrahot gas-giant exoplanet with a stratosphere, Nature 548 (2017) 58–61. doi:10.1038/nature23266.
- [26] S. R. Merritt, N. P. Gibson, S. K. Nugroho, E. J. W. de Mooij, M. J. Hooton, S. M. Matthews, L. K. McKemmish, T. Mikal-Evans, N. Nikolov, D. K. Sing, J. J. Spake, C. A. Watson, Non-detection of TiO and VO in the atmosphere of WASP-121b using high-resolution spectroscopy, Astron. Astrophys. 636 (2020) A117. doi:10.1051/0004-6361/201937409.
- [27] J. M. Goyal, N. Mayne, B. Drummond, D. K. Sing, E. Hebrard, N. Lewis, P. Tremblin, M. W. Phillips, T. Mikal-Evans, H. R. Wakeford, A library of self-consistent simulated exoplanet atmospheres, Mon. Not. R. Astron. Soc. 498 (2020) 4680–4704. doi:10.1093/mnras/staa2300.
- [28] J.-M. Désert, A. Vidal-Madjar, A. Lecavelier des Etangs, D. Sing, D. Ehrenreich, G. Hébrard, R. Ferlet, TiO and VO broad band absorption features in the optical spectrum of the atmosphere of the hot-Jupiter HD 209458b, Astron. Astrophys. 492 (2008) 585–592. doi: 10.1051/0004-6361:200810355.
- [29] H. Schwarz, M. Brogi, R. de Kok, J. Birkby, I. Snellen, Evidence against a strong thermal inversion in HD 209458b from high-dispersion spectroscopy, Astron. Astrophys. 576 (2015) A111. doi:10.1051/ 0004-6361/201425170.
- [30] L. K. McKemmish, S. N. Yurchenko, J. Tennyson, ExoMol Molecular linelists – XVIII. The spectrum of Vanadium Oxide, Mon. Not. R. Astron. Soc. 463 (2016) 771–793. doi:10.1093/mnras/stw1969.
- [31] S. N. Yurchenko, L. Lodi, J. Tennyson, A. V. Stolyarov, Duo: A general program for calculating spectra of diatomic molecules, Comput. Phys. Commun. 202 (2016) 262 – 275. doi:10.1016/j.cpc.2015.12.021.
- [32] L. K. McKemmish, S. N. Yurchenko, J. Tennyson, Ab initio calculations to support accurate modelling of the rovibronic spectroscopy calculations of vanadium monoxide (VO), Mol. Phys. 114 (2016) 3232–3248. doi: 10.1080/00268976.2016.1225994.
- [33] S. de Regt, A. Y. Kesseli, I. A. G. Snellen, S. R. Merritt, K. L. Chubb, A quantitative assessment of the VO line list: Inaccuracies hamper highresolution VO detections in exoplanet atmospheres, arXiv e-prints (2022) arXiv:2203.03585arXiv:2203.03585.
- [34] W. S. Hopkins, S. M. Hamilton, S. R. Mackenzie, The electronic spectrum of vanadium monoxide across the visible: New bands and new insight, J. Chem. Phys. 130 (2009) 144308. doi:10.1063/1.3104844.

- [35] D. Richards, R. F. Barrow, Nuclear Hyperfine Interactions in Diatomic Molecules and the Ground State of VO, Nature 217 (1968) 842. doi: 10.1038/217842a0.
- [36] A. J. Merer, Spectroscopy of the diatomic 3d transition-metal oxides, Ann. Rev. Phys. Chem. 40 (1989) 407–438. doi:10.1146/annurev.pc.40. 100189.002203.
- [37] T. Furtenbacher, A. G. Császár, J. Tennyson, MARVEL: measured active rotational-vibrational energy levels, J. Mol. Spectrosc. 245 (2007) 115– 125. doi:10.1016/j.jms.2007.07.005.
- [38] T. Furtenbacher, A. G. Császár, MARVEL: measured active rotational-vibrational energy levels. II. Algorithmic improvements, J. Quant. Spectrosc. Radiat. Transf. 113 (2012) 929–935. doi:10.1016/j.jqsrt.2012.01.005.
- [39] R. Tóbiás, T. Furtenbacher, J. Tennyson, A. G. Császár, Accurate empirical rovibrational energies and transitions of H₂¹⁶O, Phys. Chem. Chem. Phys. 21 (2019) 3473–3495. doi:10.1039/c8cp05169k.
- [40] A. G. Császár, T. Furtenbacher, Spectroscopic networks, J. Mol. Spectrosc. 266 (2011) 99 – 103. doi:10.1016/j.jms.2011.03.031.
- [41] R. Tobias, T. Furtenbacher, I. Simko, A. G. Csaszar, M. L. Diouf, F. M. J. Cozijn, J. M. A. Staa, E. J. Salumbides, W. Ubachs, Spectroscopic-network-assisted precision spectroscopy and its application to water, Nature Comms. 11 (2020) 1708. doi: 10.1038/s41467-020-15430-6}.
- [42] A. R. Al-Derzi, S. N. Yurchenko, J. Tennyson, M. Melosso, N. Jiang, C. Puzzarini, L. Dore, T. Furtenbacher, R. Tobias, A. G. Császár, MARVEL analysis of the measured high-resolution spectra of formaldehyde, J. Quant. Spectrosc. Radiat. Transf. 266 (2021) 107563. doi: 10.1016/j.jgsrt.2021.107563.
- [43] A. S.-C. Cheung, R. C. Hansen, A. J. Merer, Laser spectroscopy of VO: Analysis of the rotational and hyperfine structure of the C $^4\Sigma^-$ X $^4\Sigma^-$ (0, 0) band, J. Mol. Spectrosc. 91 (1982) 165–208. doi: 10.1016/0022-2852(82)90039-X.
- [44] M. A. Flory, L. M. Ziurys, Submillimeter-wave spectroscopy of VN ($X^3\Delta_r$) and VO ($X^4\Sigma^-$): A study of the hyperfine interactions, J. Mol. Spectrosc. 247 (2008) 76–84. doi:10.1016/j.jms.2007.09.007.
- [45] A. G. Adam, M. Barnes, B. Berno, R. D. Bower, A. J. Merer, Rotational and Hyperfine Structure in the B $^4\Pi$ –X $^4\Sigma^-$ (0,0) Band of VO at 7900 Å: Perturbations by the a $^2\Sigma^+$, v = 2 Level, J. Mol. Spectrosc. 170 (1995) 94–130. doi:10.1006/jmsp.1995.1059.
- [46] C. M. Western, PGOPHER: A program for simulating rotational, vibrational and electronic spectra, J. Quant. Spectrosc. Radiat. Transf. 186 (2017) 221–242. doi:10.1016/j.jqsrt.2016.04.010.
- [47] A. Lagerqvist, L. E. Selin, Rotationsanalyse der sichtbaren Vanadiumoxydbanden, Arkiv for Fysik 12 (1957) 553–568.
- [48] J. Tennyson, P. F. Bernath, L. R. Brown, A. Campargue, M. R. Carleer, A. G. Császár, R. R. Gamache, J. T. Hodges, A. Jenouvrier, O. V. Naumenko, O. L. Polyansky, L. S. Rothman, R. A. Toth, A. C. Vandaele, N. F. Zobov, L. Daumont, A. Z. Fazliev, T. Furtenbacher, I. E. Gordon, S. N. Mikhailenko, S. V. Shirin, IUPAC critical Evaluation of the Rotational Vibrational Spectra of Water Vapor. Part I. Energy Levels and Transition Wavenumbers for H₂¹⁷O and H₂¹⁸O, J. Quant. Spectrosc. Radiat. Transf. 110 (2009) 573–596. doi:10.1016/j.jgsrt.2009.02.014.
- [49] M. H. Beck, A. Jäckle, G. A. Worth, H. D. Meyer, The multiconfiguration time-dependent Hartree (MCTDH) method: a highly efficient algorithm for propagating wavepackets, Phys. Rep. 324 (2000) 1–105. doi:10. 1016/S0370-1573(99)00047-2.
- [50] A. Fast, S. A. Meek, Frequency comb referenced spectroscopy of A–X 0–0 transitions in SH, J. Chem. Phys. 154 (11) (2021) 114304. doi: 10.1063/5.0042552.
- [51] C. A. Bowesman, M. Shuai, S. N. Yurchenko, J. Tennyson, A high resolution line list for AIO, Mon. Not. R. Astron. Soc. 508 (2021) 3181–3193. doi:10.1093/mnras/stab2525.
- [52] R. L. Cook, F. C. De Lucia, Application of the Theory of Irreducible Tensor Operators to Molecular Hyperfine Structure, American Journal of Physics 39 (1971) 1433–1454. doi:10.1119/1.1976693.
- [53] R. N. Zare, Angular Momentum: Understanding Spatial Aspects in Chemistry and Physics, Wiley, 1988.
- [54] J. M. Brown, A. Carrington, Rotational Spectroscopy of Diatomic Molecules, Cambridge University Press, 2003. doi:10.1017/ CB09780511814808.
- [55] P. Bunker, P. Jensen, Molecular Symmetry and Spectroscopy, NRC Research Press, 2006.

- [56] R. D. Suenram, G. T. Fraser, F. J. Lovas, C. W. Gillies, Microwave spectra and electric dipole moments of X $^4\Sigma_{12}^-$ VO and NbO, J. Mol. Spectrosc. 148 (1991) 114–122. doi:10.1016/0022-2852(91)90040-H.
- [57] K. D. Carlson, C. Moser, Electronic Ground State and Wavefunctions for Vanadium Monoxide, J. Chem. Phys. 44 (1966) 3259–3265. doi: 10.1063/1.1727221.
- [58] P. H. Kasai, ESR of VO in Argon matrix at 4 degree K: Establishment of its electronic ground state, J. Chem. Phys. 49 (1968) 4979. doi: 10.1063/1.1669987.
- [59] L. Veseth, Fine-structure of 4-PI states in diatomic-molecules, Phys. Scr. 12 (1975) 125–128. doi:10.1088/0031-8949/12/3/004.
- [60] C. W. Bauschlicher, S. R. Langhoff, Theoretical-studies of the low-lying states of ScO, ScS, VO, and VS, J. Chem. Phys. 85 (1986) 5936–5942. doi:10.1063/1.451505.
- [61] M. Dolg, U. Wedig, H. Stoll, H. Preuss, Ab initio pseudopotential study of the 1st row transition-metal monoxides and iron monohydride, J. Chem. Phys. 86 (1987) 2123–2131. doi:10.1063/1.452110.
- [62] A. J. Bridgeman, J. Rothery, Periodic trends in the diatomic monoxides and monosulfides of the 3d transition metals, J. Chem. Soc. Dalton (2000) 211–218doi:10.1039/a906523g.
- [63] M. Calatayud, B. Silvi, J. Andres, A. Beltran, A theoretical study on the structure, energetics and bonding of VO_x and VO_x (x=1-4) systems, Chem. Phys. Lett. 333 (2001) 493–503. doi:10.1016/S0009-2614(00) 01287-2.
- [64] E. Broclawik, T. Borowski, Time-dependent DFT study on electronic states of vanadium and molybdenum oxide molecules, Chem. Phys. Lett. 339 (2001) 433–437. doi:10.1016/S0009-2614(01)00361-X.
- [65] M. Pykavy, C. van Wullen, Multireference correlation calculations for the ground states of VO^{+/0/-} using correlation consistent basis sets, J. Phys. Chem. A 107 (2003) 5566–5572. doi:10.1021/jp027264n.
- [66] W. C. Mackrodt, D. S. Middlemiss, T. G. Owens, Hybrid density functional theory study of vanadium monoxide, Phys. Rev. B 69 (2004) 115119. doi:10.1103/PhysRevB.69.115119.
- [67] D. Quan, W. Ling, S. Xiao-Hong, G. Tao, Study on potential energy functions and spectrum constants of VO^{n±} (n=0, 1, 2), Acta Phys. Sin. 55 (2006) 6308–6314. doi:10.7498/aps.55.6308.
- [68] E. Miliordos, A. Mavridis, Electronic structure of vanadium oxide. Neutral and charged species, VO^{0,±}, J. Phys. Chem. A 111 (2007) 1953–1965. doi:10.1021/jp067451b.
- [69] D. Quan, W. Ling, S. Xiao-Hong, W. Hong-Yan, G. Tao, Z. Zheng-He, Study of the structures and stabilities of the VO_X (x=1 approximate to 5) molecules by density functional theory, Acta Chim. Sin. 66 (2008) 23–30.
- [70] E. L. Uzunova, H. Mikosch, G. S. Nikolov, Electronic structure of oxide, peroxide, and superoxide clusters of the 3d elements: A comparative density functional study, J. Chem. Phys. 128 (2008) 094307. doi:10.1063/1.2831583
- [71] H. J. Kulik, N. Marzari, Systematic study of first-row transition-metal diatomic molecules: A self-consistent DFT plus U approach, J. Chem. Phys. 133 (2010) 114103. doi:10.1063/1.3489110.
- [72] O. Hübner, J. Hornung, H.-J. Himmel, The electronic structure of VO in its ground and electronically excited states: A combined matrix isolation and quantum chemical (MRCI) study, J. Chem. Phys. 143 (2015) 024309. doi:10.1063/1.4926393.
- [73] A. S. Gentleman, A. Iskra, H. Köckert, S. R. Mackenzie, Photodissociation dynamics and the dissociation energy of vanadium monoxide, VO, investigated using velocity map imaging, Phys. Chem. Chem. Phys. 21 (2019) 15560–15567, doi:10.1039/C9CP02120E.
- [74] D. M. Merriles, A. Sevy, C. Nielson, M. D. Morse, The bond dissociation energy of VO measured by resonant three-photon ionization spectroscopy, J. Chem. Phys. 153 (2020) 024303. doi:10.1063/5.0014006.
- [75] T. Jiang, Y. Chen, N. A. Bogdanov, E. Wang, A. Alavi, J. Chen, A full configuration interaction quantum Monte Carlo study of ScO, TiO, and VO molecules, J. Chem. Phys. (2021) 164302doi:10.1063/5.0046464.
- [76] P. C. Mahanti, The Band Spectrum Of Vanadium Oxide, Proc. Phys. Soc. 47 (1935) 433.
- [77] A. Lagerqvist, L. E. Selin, Some infrared bands of vanadium oxide, Arkiv for Fysik 11 (1957) 429–430.
- [78] D. Richards, R. F. Barrow, New Type of Perturbation caused by a Magnetic Hyperfine Interaction, observed in the Ground State of VO, Nature 219 (1968) 1244–1245. doi:10.1038/2191244a0.
- [79] B. B. Laud, D. R. Kalsulka, Emission spectrum of VO molecule, Indian

- J. Phys. 42 (1968) 61-71.
- [80] J. M. Dyke, B. W. J. Gravenor, M. P. Hastings, A. Morris, High-temperature photoelectron-spectroscopy: The vanadium monoxide molecule, J. Phys. Chem. 89 (1985) 4613–4617. doi:10.1021/ i100267a040.
- [81] A. S.-C. Cheung, R. C. Hansen, A. M. Lyyra, A. J. Merer, A novel electronic-hyperfine perturbation in the C $^4\Sigma^-$ state of VO, J. Mol. Spectrosc. 86 (1981) 526–533. doi:10.1016/0022-2852(81)90298-8.
- [82] A. S.-C. Cheung, A. W. Taylor, A. J. Merer, Fourier transform spectroscopy of VO: Rotational structure in the A $^4\Pi$ -X $^4\Sigma$ ⁻ system near 10 500 Å, J. Mol. Spectrosc. 92 (1982) 391–409. doi:10.1016/0022-2852(82) 90110-2
- [83] W. H. Hocking, A. J. Merer, D. J. Milton, Resolved hyperfine structure in the C–X electronic transition of VO. An internal hyperfine perturbation in the C ⁴Σ⁻ state, Can. J. Phys. 59 (1981) 266–270. doi:10.1139/ p81-035.
- [84] A. J. Merer, G. Huang, A. S.-C. Cheung, A. W. Taylor, New quartet and doublet electronic transitions in the near-infrared emission spectrum of VO, J. Mol. Spectrosc. 125 (1987) 465–503. doi:10.1016/ 0022-2852(87)90110-X.
- [85] A. S.-C. Cheung, P. G. Hajigeorgiou, G. Huang, S. Z. Huang, A. J. Merer, Rotational Structure and Perturbations in the B ⁴Π–X ⁴Σ[−] (1, 0) Band of VO, J. Mol. Spectrose. 163 (1994) 443–458. doi:10.1006/jmsp.1994. 1039.
- [86] L. Karlsson, B. Lindgren, C. Lundevall, U. Sassenberg, Lifetime Measurements of the A ⁴Π, B ⁴Π, and C ⁴Σ⁻ States of VO, J. Mol. Spectrosc. 181 (1997) 274–278. doi:10.1006/jmsp.1996.7173.
- [87] R. S. Ram, P. F. Bernath, S. P. Davis, A. J. Merer, Fourier Transform Emission Spectroscopy of a New ²Φ-1 ²Δ System of VO, J. Mol. Spectrosc. 211 (2002) 279–283. doi:10.1006/jmsp.2001.8510.
- [88] R. S. Ram, P. F. Bernath, Emission spectroscopy of a new ² Δ-1 ² Δ system of VO, J. Mol. Spectrosc. 229 (2005) 57–62. doi:10.1016/j.jms. 2004.08.014.
- [89] Q. Qu, S. N. Yurchenko, J. Tennyson, Hyperfine-resolved variational nuclear motion spectra of diatomic molecules, J. Chem. Theory Comput. 18 (2022) 1808–1820. doi:10.1021/acs.jctc.1c01244.
- [90] P. Sriramachandran, S. P. Bagare, N. Rajamanickam, K. Balachandrakumar, Presence of LaO, ScO and VO Molecular Lines in Sunspot Umbral Spectra, Sol. Phys. 252 (2008) 267–281. doi:10.1007/s11207-008-9261-1.
- [91] J. Tennyson, P. F. Bernath, L. R. Brown, A. Campargue, M. R. Carleer, A. G. Császár, L. Daumont, R. R. Gamache, J. T. Hodges, O. V. Naumenko, O. L. Polyansky, L. S. Rothman, R. A. Toth, A. C. Vandaele, N. F. Zobov, A. Z. Fazliev, T. Furtenbacher, I. E. Gordon, S. N. Mikhailenko, B. A. Voronin, IUPAC critical Evaluation of the Rotational-Vibrational Spectra of Water Vapor. Part II. Energy Levels and Transition Wavenumbers for HD¹⁶O, HD¹⁷O, and HD¹⁸O, J. Quant. Spectrosc. Radiat. Transf. 111 (2010) 2160–2184. doi:10.1016/j.jgsrt.2010.06.012.
- [92] S. N. Yurchenko, H. Williams, P. C. Leyland, L. Lodi, J. Tennyson, ExoMol line lists XXVIII: The rovibronic spectrum of AlH, Mon. Not. R. Astron. Soc. 479 (2018) 1401–1411. doi:10.1093/mnras/sty1524.
- [93] D. Darby-Lewis, H. Shah, D. Joshi, F. Khan, M. Kauwo, N. Sethi, P. F. Bernath, T. Furtenbacher, R. Tobias, A. G. Csaszar, J. Tennyson, MARVEL analysis of the measured high-resolution spectra of NH, J. Mol. Spectrosc. 362 (2019) 69–76. doi:10.1016/j.jms.2019.06.002.
- [94] T. Furtenbacher, S. T. Hegedus, J. Tennyson, A. G. Császár, Analysis of the measured high-resolution doublet rovibronic spectra of ¹²CH and ¹⁶OH, Phys. Chem. Chem. Phys. (2022).

The authors declare they have no conflict of interest.

